

# Glimpses of the $X_{17}$ from coherent elastic neutrino nucleus scattering

J. Rathsman<sup>1\*</sup>, J. Cederkäll<sup>1†</sup>, Y. Hiçyılmaz<sup>2,3,4‡</sup>, E. Lytken<sup>1§</sup>, S. Moretti<sup>3,4¶</sup>

<sup>1</sup> *Department of Physics, Lund University,  
221 00 Lund, Sweden*

<sup>2</sup> *Department of Physics, Balıkesir University,  
TR10145, Balıkesir, Turkey*

<sup>3</sup> *Department of Physics and Astronomy, Uppsala University,  
751 20, Uppsala, Sweden*

<sup>4</sup> *School of Physics and Astronomy, University of Southampton  
Highfield, Southampton SO17 1BJ, United Kingdom*

March 23, 2026

## Abstract

We show that the process of Coherent Elastic neutrino ( $\nu$ ) Nucleus Scattering ( $CE\nu NS$ ) at nuclear reactor experiments has significant sensitivity to the so-called  $X_{17}$  particle, which has been invoked to explain the ATOMKI anomaly, wherein electron-positron pairs emerging from a nuclear transition of excited  ${}^8\text{Be}$ ,  ${}^4\text{He}$  and  ${}^{12}\text{C}$  nuclei are studied. Such a new state has potentially been identified as a spin-1 object, with axial-vector couplings and a mass around 16.7 MeV, hence, in the kinematic range accessible by the aforementioned experimental settings. Specifically, we fit CONUS+ and Dresden-II data and show that a robust statistical analysis renders these more compatible with the  $X_{17}$  hypothesis, in turn interfering with the Standard Model (SM), than with that of the latter alone. The same stays true when also adding COHERENT data from  $\pi^+$  decays at rest, singling out two regions of preferred couplings of the  $X_{17}$  to electron and muon neutrinos as well as nuclei.

---

\*Corresponding author, e-mail: johan.rathsman@fysik.lu.se

†E-mail: joakim.cederkall@fysik.lu.se

‡E-mail: yasarhicyilmaz@balikesir.edu.tr; y.hicyilmaz@physics.uu.se; y.hicyilmaz@soton.ac.uk

§E-mail: else.lytken@fysik.lu.se

¶E-mail: stefano.moretti@physics.uu.se; s.moretti@soton.ac.uk

# 1 Introduction

The physics of Coherent Elastic Neutrino ( $\nu$ ) Nucleus Scattering ( $\text{CE}\nu\text{NS}$ ) at reactors involves the scattering of neutrinos off atomic nuclei, which is a key process for probing both Standard Model (SM) and Beyond the SM (BSM) interactions. Indeed,  $\text{CE}\nu\text{NS}$  was confirmed experimentally in 2017 by the COHERENT collaboration [1], with secondary neutrinos produced by the Spallation Neutron Source (SNS) at the Oak Ridge National Laboratory (ORNL). The first measurement of  $\text{CE}\nu\text{NS}$  using reactor anti-neutrinos was done at the Dresden-II reactor [2] and subsequently it has been confirmed by the CONUS+ collaboration [3] in 2025. Reactors are a high constant flux source of low-energy (a few MeV) electron anti-neutrinos, whereas the spallation sources produce higher-energy (tens of MeV), pulsed and multi-flavour beams. In addition to precision neutrino measurements, neutrino beams from reactors can also be used to search for new low-mass gauge bosons, e.g., emerging from  $U(1)'$  theories.

In particular, amongst such  $U(1)'$  frameworks, we will single out here a specific one embedding a state which could be identified as the so-called  $X_{17}$  particle explaining the ATOMKI anomaly [4–13]. The ATOMKI experiment at the Hungarian Institute for Nuclear Research (HUN-REN) in Debrecen [14] has studied over the past few years the properties of  $e^+e^-$  pairs generated during nuclear transitions of  $^8\text{Be}$ ,  $^4\text{He}$  and  $^{12}\text{C}$  nuclei [4–13]. An excess in both their invariant mass and opening angle was consistently detected at more than  $5\sigma$  level (when combined across all chemical elements), corresponding to the possibility of a new particle (the aforementioned  $X_{17}$ ) with a mass at approximately 16.7 MeV. Additional evidence of the  $X_{17}$  has emerged also from an independent experiment hosted at VNU University of Science in Hanoi, which reported replicating the ATOMKI anomaly in early 2024, seen through the observation of an anomaly in the angular distribution in the case of  $^8\text{Be}$  [15].

The PADME experiment at the Laboratori Nazionali di Frascati (LNF) also showed sensitivity to this mass and has recently posted their results in Ref. [16], claiming a  $2\sigma$  excess in correspondence of the mass indicated by the ATOMKI experiment. In contrast, the MEG-II experiment at the Paul Scherrer Institut (PSI) in Villigen appears to disfavour the  $X_{17}$  hypothesis and has set an upper limit on the  $e^+e^-$  decay rate of such a possible new particle [17]. Other facilities also have sensitivity to a possible  $X_{17}$  state, including those at CERN (the NA62 and nTOF experiments), PSI (the Mu3e experiment), JLab (the PRad, DarkLight and HPS experiment) and GANIL (the New JEDI project), yet, none of those already operating has reported conclusive arguments in either direction [18].

Interpretations of the  $X_{17}$  have been numerous in literature<sup>1</sup>. Of all these, we embrace in this paper the one assuming that the  $X_{17}$  is a spin-1 boson, which could well (but not necessarily) be the carrier of a postulated fifth force, potentially connected with a dark sector, itself containing a Dark Matter (DM) candidate. In fact, Ref. [19] (see [20–28] for alternative interpretations) proved that, in the case of a pure vector coupling, the new boson should be protophobic, as implied primarily by the NA48/2 and NA64 data [29,30]. Further phenomenological studies [31–33] showed that, due to absence of bremsstrahlung radiation of the  $X_{17}$  and conflicts with the non-observation of deviations from the SM in neutrino scattering experiments, the theoretical frameworks including a pure vector mediator are less likely, while an axial-vector state appears as the best candidate to comply with the above restrictions while simultaneously partake in the  $X_{17}$  hypothesis [18].

---

<sup>1</sup>See <https://cerncourier.com/a/mixed-signals-from-x17/> for a recent popularised account of the ATOMKI anomaly, including a concise review of its possible explanations.

In addition, several analyses have been conducted to investigate the effects of such a light  $X_{17}$  also on the anomalous magnetic moment of the electron ( $a_e$ ) and muon ( $a_\mu$ ) as well as at the Large Hadron Collider (LHC), including flavour observables (such as  $R_{K^{(*)}}$ ) [23, 24, 34–39], all pointing presently to the  $X_{17}$  consistency with all such datasets (and the possibility of its detection in the future). This is all the more intriguing as attempts to interpret the ATOMKI results in terms of background effects have demonstrated that nuclear physics or QCD cannot lead to a satisfactory explanation [40–47].

A minimal theoretical approach embedding the  $X_{17}$  is given by a family-dependent  $U(1)$  extension of the SM, which breaking introduces a new light vector boson, effectively a  $Z'$ , which can indeed be interpreted as the  $X_{17}$ , as first introduced in Ref. [48]. This naturally allows for axial-vector couplings, depending on the gauge quantum numbers involved. Furthermore, in this framework, the Yukawa interactions are suitably modified by higher-dimensional operators [49]. This setup is what we will pursue in the present paper. We also note that, in a recent study, a  $X_{17}$  with both vector and axial vector couplings has been put forward although that particular realisation was found to be in tension with constraints from atomic parity violation [50].

Notice, in particular, that this scenario does not prevent the  $X_{17}$  from coupling to neutrinos, so that it can also lead to Non-Standard Interactions (NSIs) of the latter affecting neutrino flavour ratios in matter [51]. Therefore, the ensuing experimental constraints on NSIs from neutrino oscillations can be applied to restrict the family dependent (non-universal) couplings of the new boson to SM fermions, as recently done (using data from TEXONO [52, 53] and IceCube [54]) in Ref. [55]. Indeed, the allowed possibility of the  $X_{17}$  coupling to neutrinos, recently prompted us to study, in the spirit of Ref. [56], the possibilities to discover this object in  $CE\nu NS$  at the European Spallation Source (ESS) in Lund, building on the work done in Refs. [57, 58]. In fact, as already intimated, similar results via  $CE\nu NS$  may also be obtained through the SNS at the ORNL in the aforementioned COHERENT experiment [59–63]<sup>2</sup>.

The  $CE\nu NS$  process was first suggested by Freedman already in 1973 [64], but the small nuclear recoil energies involved meant that it was not experimentally confirmed until 2017, indeed, by the COHERENT collaboration [1]. Apart from confirming the phenomenon itself,  $CE\nu NS$  can also be used to study both the SM, including the neutron skin effect in nuclei and the neutrino charge radius (see [65] for an early example), as well as BSM physics (especially when its mass states are in the sub-GeV range) [66]. In particular, light vector bosons such as the  $X_{17}$  can contribute to the cross-section both through constructive and destructive interference with the  $\gamma$  and  $Z$  bosons of the SM. Until our recent study [57, 58], only flavour universal models, e.g., the  $B - L$  one, where the couplings to electron and muon neutrinos are the same, have been considered [67–72].

With the advent of  $CE\nu NS$  measurements from the nuclear reactor experiments Dresden-II [2] and CONUS+ [3], these data have also been included in the BSM analyses of Refs. [73–77], although, as pointed out in [78], there is some tension between the data from Dresden-II and CONUS+ when analysed in the SM. Very recently, also the impact of light mediators contributing through  $CE\nu NS$  to DM direct detection experiments, using data from XENON [79] and PandaX [80], has been analysed [81, 82]. On a related note, reactor data from  $CE\nu NS$  has also been used to improve the determination of the neutrino mass ordering [83]. For a brief review of the physics of  $CE\nu NS$  we refer to [84].

In the light of the strong sensitivity to the  $X_{17}$  displayed by  $CE\nu NS$  experiments, we have

---

<sup>2</sup>See <https://indico.cern.ch/event/1439855/contributions/6461655/>.

revisited here the possibilities in this context offered by nuclear reactor experiments such as Dresden-II and CONUS+ as well as others (TEXONO [85],  $\nu$ GEN [86], NUCLEUS [87], NEON [88], CONNIE [89]) which are in the planning or have not yet made any observations, thereby complementing the aforementioned accelerator-based efforts, wherein abundant anti-neutrinos beams from fission processes can probe a variety of BSM scenarios, e.g., including sterile neutrinos, DM and others.

The layout of our paper is as follows. In the next section we introduce our BSM framework, including a description of its implementation in numerical tools. Then we proceed to describe the theory of CE $\nu$ NS in nuclear reactors Sect. 3, where we also discuss the experimental setups (in particular, those in Dresden-II and CONUS+) which show sensitivity already at present to the  $X_{17}$ , including interpreting their data in combination with those from SNS processes. (The technical details of our treatment of the COHERENT detector performance in carrying out the data combination discussed above, are left for an Appendix.) We finally conclude in Sect. 4.

## 2 The theoretical framework embedding the $X_{17}$

In the following we give a brief description of the minimal extension of the SM with a generic  $U(1)'$  gauge group studied in this work. For more details of the model we refer to [57]. The kinetic terms in the Lagrangian that depend on the hypercharge group of the SM,  $U(1)_Y$ , and the additional gauge structure,  $U(1)'$ , are given by

$$\mathcal{L}_{\text{Kin}}^{U(1)'} = -\frac{1}{4}\hat{F}_{\mu\nu}\hat{F}^{\mu\nu} - \frac{1}{4}\hat{F}'_{\mu\nu}\hat{F}'^{\mu\nu} - \frac{\eta}{2}\hat{F}'_{\mu\nu}\hat{F}^{\mu\nu}, \quad (2.1)$$

where the field strengths  $\hat{F}_{\mu\nu}$  and  $\hat{F}'_{\mu\nu}$  correspond to the gauge fields  $\hat{B}_\mu$  and  $\hat{B}'_\mu$  of  $U(1)_Y$  and  $U(1)'$ , respectively, while the parameter  $\eta$  quantifies the kinetic mixing between these Abelian symmetries. The gauge covariant derivative is written as

$$\mathcal{D}_\mu = \partial_\mu + \dots + ig_1 Y B_\mu + i(\tilde{g}Y + g'Q')B'_\mu, \quad (2.2)$$

where  $Y$  represents the hypercharge with coupling  $g_1$  while  $Q'$  denotes the  $U(1)'$  charge with associated coupling  $g' = \hat{g}'/\sqrt{1-\eta^2}$ , where  $\hat{g}'$  is the original  $U(1)'$  coupling before the transformation of the gauge fields for diagonalisation, while  $\tilde{g} = -\eta g_1/\sqrt{1-\eta^2}$  characterises the strength of the gauge mixing between  $U(1)_Y$  and  $U(1)'$ .

In the model, a new SM singlet complex scalar  $\chi$  breaks the  $U(1)'$  symmetry spontaneously through a Vacuum Expectation Value (VEV)  $\langle\chi\rangle = v'/\sqrt{2}$ . A new massive vector boson is generated by such a breaking of the  $U(1)'$ . The neutral gauge boson mass eigenstates in the model are obtained through the rotation:

$$\begin{pmatrix} B^\mu \\ W_3^\mu \\ B'^\mu \end{pmatrix} = \begin{pmatrix} \cos\theta_W & -\sin\theta_W \cos\theta' & \sin\theta_W \sin\theta' \\ \sin\theta_W & \cos\theta_W \cos\theta' & -\cos\theta_W \sin\theta' \\ 0 & \sin\theta' & \cos\theta' \end{pmatrix} \begin{pmatrix} A^\mu \\ Z^\mu \\ Z'^\mu \end{pmatrix}, \quad (2.3)$$

where  $\theta_W$  is the Weinberg angle and  $\theta'$  is the  $Z - Z'$  mixing angle [90]:

$$\tan 2\theta' = \frac{2g_H g_Z}{g_H^2 + (2Q'_\chi g' v'/v)^2 - g_Z^2}, \quad (2.4)$$

with  $Q'_\chi$  being the  $U(1)'$  charge of the  $\chi$ -field,  $g_H = \tilde{g} + 2g'Q'_H$  and  $g_Z = \sqrt{g_2^2 + g_1^2}$  is the Electro-Weak (EW) coupling.

The mixing angle  $\theta'$  is constrained by the LEP precision measurements to be such that  $|\theta'| < 10^{-3}$  [91, 92]. In the small  $\theta'$  approximation, the  $Z$  and  $Z'$  masses can be written as

$$m_Z^2 \simeq \frac{v^2}{4} g_Z^2, \quad m_{Z'}^2 \simeq (Q'_\chi g' v')^2, \quad (2.5)$$

while the mixing angle simplifies to

$$\theta' \simeq -\frac{g_H}{g_Z}, \quad (2.6)$$

where  $g_H^2 \ll g_Z^2$  and  $(g'v')^2 \ll (g_Z v)^2$  have also been assumed. For  $g' \sim \mathcal{O}(10^{-4} - 10^{-5})$ ,  $M_{Z'}$  becomes light ( $\mathcal{O}(10)$  MeV) when  $v' \approx \mathcal{O}(100 - 1000)$  GeV, then potentially offering a candidate to address the ATOMKI anomaly.

The  $Z'$  interaction Lagrangian with SM fermions is

$$\begin{aligned} \mathcal{L}^{Z'} &= \bar{q}\gamma^\mu \left( C_L^{qq'} P_L + C_R^{qq'} P_R \right) q' Z'_\mu + \bar{\nu}_l \gamma^\mu \left( C_L^{ll'} P_L \right) \nu_{l'} Z'_\mu \\ &+ \bar{l} \gamma^\mu \left( C_L^{ll'} P_L + C_R^{ll'} P_R \right) l' Z'_\mu, \end{aligned} \quad (2.7)$$

where  $q^{(\prime)}$ ,  $l^{(\prime)}$  and  $\nu_{l^{(\prime)}}$  refer to up-type/down-type quarks, charged leptons and their neutrinos while  $C_L^{XX}$  and  $C_R^{XX}$  are Left ( $L$ ) and Right ( $R$ ) handed couplings, respectively, with  $P_L$  and  $P_R$  the corresponding projection operators  $\frac{1 \mp \gamma^5}{2}$ , respectively. In the model, we assume a flavour-conserving scenario for the quark and lepton sectors. Then, the diagonal couplings are

$$C_L^{ff} = -g_Z \sin \theta' (T_f^3 - \sin^2 \theta_W Q_f) + (\tilde{g} Y_{f,L} + g' Q'_{f,L}) \cos \theta', \quad (2.8)$$

$$C_R^{ff} = g_Z \sin^2 \theta_W \sin \theta' Q_f + (\tilde{g} Y_{f,R} + g' Q'_{f,R}) \cos \theta', \quad (2.9)$$

where  $T_f^3$  and  $Q_f$  are the fermion's weak isospin and electric charge, respectively, with  $Y_{f,L/R}$  and  $Q'_{f,L/R}$  being the  $U(1)_Y$  and  $U(1)'$  charges.

As for the vector and axial couplings, these are defined as

$$C_{f,V} = \frac{C_R^{ff} + C_L^{ff}}{2}, \quad C_{f,A} = \frac{C_R^{ff} - C_L^{ff}}{2}. \quad (2.10)$$

In the limit of small gauge coupling and mixing,  $g', \tilde{g} \ll 1$ , the vector and axial couplings are found as [26]

$$\begin{aligned} C_{f,V} &\simeq \tilde{g} \cos^2 \theta_W Q_f + g' [Q'_H (T_f^3 - 2 \sin^2 \theta_W Q_f) + (Q'_{f,R} + Q'_{f,L})/2], \\ C_{f,A} &\simeq g' [-Q'_H T_f^3 + (Q'_{f,R} - Q'_{f,L})/2]. \end{aligned} \quad (2.11)$$

Concerning the Yukawa sector of the SM Lagrangian, this reads as:

$$-\mathcal{L}_{\text{Yuk.}}^{\text{SM}} = Y_u \bar{Q} \tilde{H} u_R + Y_d \bar{Q} H d_R + Y_e \bar{L} H e_R. \quad (2.12)$$

For the  $U(1)'$  charges satisfying the gauge invariance conditions in such a Yukawa sector, axial-vector  $Z'$  couplings for quarks and charged leptons vanish. The experimental results

put very stringent constraints on a pure vector  $X_{17}$ . Instead, our model introduces flavour-dependent  $U(1)'$  charges to generate crucial axial-vector couplings with nucleons, evading experimental constraints [19, 20, 29]. The model provides this through a mechanism where only third-generation fermions obtain masses via SM-like Yukawa terms while the first- and second-generation masses arise from higher-dimensional operators:

$$\begin{aligned}
-\mathcal{L}_{\text{Yukawa}} &= \Gamma_i^u \left( \frac{\chi^*}{M} \right)^{n_i} \bar{Q}_{L,i} \tilde{H} u_{R,i} + \Gamma_i^d \left( \frac{\chi}{M} \right)^{l_i} \bar{Q}_{L,i} H d_{R,i} \\
&+ \Gamma_i^e \left( \frac{\chi}{M} \right)^{m_i} \bar{L}_i H e_{R,i} + h.c., \quad i = 1, 2,
\end{aligned} \tag{2.13}$$

where  $M$  sets the non-renormalisable scale and we assume that the couplings are flavour diagonal in order to avoid tree level flavour changing neutral currents. The requirement of gauge invariance under the  $U(1)'$  symmetry then gives

$$\begin{aligned}
-n_{1,2} Q'_\chi - Q'_{Q_{1,2}} - Q'_H + Q'_{u_{1,2}} &= 0, \\
l_{1,2} Q'_\chi - Q'_{Q_{1,2}} + Q'_H + Q'_{d_{1,2}} &= 0, \\
m_{1,2} Q'_\chi - Q'_{L_{1,2}} + Q'_H + Q'_{e_{1,2}} &= 0,
\end{aligned} \tag{2.14}$$

which will generate non-zero axial couplings when  $n_i$ ,  $m_i$  or  $l_i \neq 0$ . In the following, as intimated, we assume flavour-universality of the first two generations of  $U(1)'$  quark charges ( $Q'_{Q_1} = Q'_{Q_2}$  etc.), whereas the lepton charges are fully non-universal. As a consequence we will have  $n_1 = n_2$  and  $l_1 = l_2$ . The  $U(1)'$  charges must also satisfy the anomaly cancellation conditions for the SM fermions as well as additional  $R$ -handed neutrinos:

$$\sum_{i=1}^3 (2Q'_{Q_i} - Q'_{u_i} - Q'_{d_i}) = 0, \tag{2.15}$$

$$\sum_{i=1}^3 (3Q'_{Q_i} + Q'_{L_i}) = 0, \tag{2.16}$$

$$\sum_{i=1}^3 \left( \frac{Q'_{Q_i}}{6} - \frac{4}{3} Q'_{u_i} - \frac{Q'_{d_i}}{3} + \frac{Q'_{L_i}}{2} - Q'_{e_i} \right) = 0, \tag{2.17}$$

$$\sum_{i=1}^3 (Q'^2_{Q_i} - 2Q'^2_{u_i} + Q'^2_{d_i} - Q'^2_{L_i} + Q'^2_{e_i}) = 0, \tag{2.18}$$

$$\sum_{i=1}^3 (6Q'^3_{Q_i} - 3Q'^3_{u_i} - 3Q'^3_{d_i} + 2Q'^3_{L_i} - Q'^3_{e_i}) + \sum_{i=1}^3 Q'^3_{\nu_i} = 0, \tag{2.19}$$

$$\sum_{i=1}^3 (6Q'_{Q_i} - 3Q'_{u_i} - 3Q'_{d_i} + 2Q'_{L_i} - Q'_{e_i}) + \sum_{i=1}^3 Q'_{\nu_i} = 0. \tag{2.20}$$

(Further information about the general charge solutions of our model can be found in Ref. [57].)

As already mentioned, in addition to the SM Higgs sector, our model includes the new complex scalar  $\chi$  whose VEV is responsible for spontaneous symmetry breaking of the  $U(1)'$  symmetry. The scalar potential of the model is given by

$$V(H, \chi) = -\mu^2 |H|^2 + \lambda |H|^4 - \mu_\chi^2 |\chi|^2 + \lambda_\chi |\chi|^4 + \kappa |\chi|^2 |H|^2, \tag{2.21}$$

| Parameter  | Scanned range                 | Parameter      | Scanned range        |
|--|-------------------------------|----------------|----------------------|
| $g'$   | $[10^{-5}, 5 \times 10^{-5}]$ | $\lambda$      | $[0.125, 0.132]$     |
| $\tilde{g}$  | $[-10^{-3}, 10^{-3}]$         | $\lambda_\chi$ | $[10^{-3}, 10^{-1}]$ |
| $v'$   | $[0.1, 1]$ TeV                | $\kappa$       | $[10^{-4}, 10^{-2}]$ |
| $Q'_{e_1}/Q'_{e_3}, Q'_{e_2}, Q'_{d_3}, Q'_H, Q'_\chi$ | $[-2, 2]$                     | $Q'_{\nu_1}$   | 0                    |
| $m_1$  | $[0, 3]$                      | $m_2$          | $[0, 3]$             |

Table 1: Scanned parameter space of the theoretical model. Note that  $m_1$  and  $m_2$  are integers and that if  $m_1 \neq m_2$  then  $Q'_{e_3}$  is a free parameter which is replaced with  $Q'_{e_1}$  if  $m_1 = m_2$ .

where  $H$  is the SM Higgs doublet and  $\kappa$  is the mixing parameter coupling the SM Higgs field to the new scalar  $\chi$ . As mentioned, this model features two physical Higgs states with two non-vanishing VEVs,  $v$  and  $v'$ , which are defined as follows:

$$\langle H \rangle = \frac{1}{\sqrt{2}} \begin{pmatrix} 0 \\ v \end{pmatrix}, \quad \langle \chi \rangle = \frac{v'}{\sqrt{2}}. \quad (2.22)$$

The physical CP-even Higgs mass eigenstates ( $h_1$  and  $h_2$ ) emerge from the interaction states  $(H, \chi)$  through an orthogonal rotation:

$$\begin{pmatrix} h_1 \\ h_2 \end{pmatrix} = \begin{pmatrix} \cos \theta & -\sin \theta \\ \sin \theta & \cos \theta \end{pmatrix} \begin{pmatrix} H \\ \chi \end{pmatrix}, \quad (2.23)$$

with the mixing angle  $\theta$  constrained to  $-\pi/2 < \theta < \pi/2$ . The corresponding mass eigenvalues are given by:

$$m_{h_{1,2}}^2 = \lambda v^2 + \lambda_\chi v'^2 \mp \sqrt{(\lambda v^2 - \lambda_\chi v'^2)^2 + (\kappa v v')^2}. \quad (2.24)$$

The mixing angle can be determined from parameters of the scalar potential via

$$\tan 2\theta = \frac{\kappa v v'}{\lambda v^2 - \lambda_\chi v'^2}. \quad (2.25)$$

Here, we assume  $h_2$  as the SM-like Higgs boson while the exotic boson  $h_1$  is lighter and dominantly a singlet-like Higgs state, which has been considered in [47] as a mediator for possible  $Z'$  signatures.

The above summarises the  $X_{17}$  model that we are considering and the free parameters of the model are given in Tab. 1, alongside their scanned ranges. To analyse the model we have implemented it using different numerical tools as follows. We have used the SPheno [93–95] and SARAH 4.14.3 [96, 97] codes in the parameter space investigation of the model. The scanning of the parameter space was performed using the Metropolis-Hastings algorithm. Moreover, we implement significant experimental constraints to our solutions. We first require the SM Higgs boson mass to be within 3 GeV of its observed value of 125 GeV and its Branching Ratios (BRs), dominated by  $\text{BR}(h_2 \rightarrow b\bar{b})$  and  $\text{BR}(h_2 \rightarrow \text{invisible})$  [*i.e.*  $h_1 h_1, Z' Z', Z Z'$ ) to be within the experimental limits [98, 99]. Then, we apply the constraints on the BRs of rare  $B$ -decays, specifically  $\text{BR}(B \rightarrow X_s \gamma)$ ,  $\text{BR}(B_s \rightarrow \mu^+ \mu^-)$  and  $\text{BR}(B_u \rightarrow \tau \nu_\tau)$  [100–102]. We have also bounded the value of the  $Z - Z'$  mixing parameter  $\theta'$  (see Eq. (2.4)) to be less than a few times  $10^{-3}$  as a result of EW precision tests [91, 92].

In the next step of the analysis, we constrain the parameter space according to the current experimental bounds on the anomalous magnetic moment results for  $(g - 2)_e$ ,  $(g - 2)_\mu$

| Observable  | Constraint   | Tolerance | Reference(s) |
|---|--|-----------|--------------|
| $m_{h_2}$   | 122 GeV – 128 GeV  |           |              |
| $\text{BR}(h_2 \rightarrow b\bar{b})$   | $> 0.4$  |           | [98]         |
| $\text{BR}(h_2 \rightarrow \text{invisible})$   | $< 0.17$   | $1\sigma$ | [99]         |
| $\text{BR}(B_s \rightarrow \mu^+\mu^-)$   | $0.8 \times 10^{-9} - 6.2 \times 10^{-9}$                                | $2\sigma$ | [101]        |
| $\text{BR}(B \rightarrow X_s \gamma)$   | $2.99 \times 10^{-4} - 3.87 \times 10^{-4}$                              | $2\sigma$ | [100]        |
| $\frac{\text{BR}(B_u \rightarrow \tau \nu_\tau)}{\text{BR}(B_u \rightarrow \tau \nu_\tau)_{\text{SM}}}$ | 0.15 – 2.41  | $3\sigma$ | [102]        |
| $\Delta a_e^{\text{Rb}}$  | $(4.8 \pm 9.0) \times 10^{-13}$  | $3\sigma$ | [105]        |
| $\Delta a_\mu$  | $(3.8 \pm 6.3) \times 10^{-9}$   | $3\sigma$ | [103, 104]   |
| $\epsilon_{ee}^\oplus - \epsilon_{\mu\mu}^\oplus$   | $[-2.26, -1.27] \cup [-0.74, 0.32]$                                      |           | [54]         |
| $\epsilon_{\tau\tau}^\oplus - \epsilon_{\mu\mu}^\oplus$   | $[-0.041, 0.042]$  |           | [54]         |
| $\sqrt{C_{e,V}^2 + C_{e,A}^2}$  | $\geq 3.6 \times 10^{-5} \times \sqrt{\text{BR}(Z' \rightarrow e^+e^-)}$ |           | [30]         |
| $\sqrt{C_{e,V} \times C_{\nu_e}}$   | $\leq 3 \times 10^{-4}$  |           | [52]         |
| $ C_{e,V} \times C_{e,A} $  | $\leq 10^{-8}$   |           | [106, 107]   |
| $ C_{e,A}  \left  \frac{188}{399} C_{u,V} + \frac{211}{399} C_{d,V} \right $                            | $\leq 1.8 \times 10^{-12}$   |           | [108, 109]   |

Table 2: Summary of the experimental constraints used.

[103–105], the related  $Z'$  couplings satisfying the ATOMKI anomaly [32], the electron beam dump experiment NA64 [30], which probes the  $Z'$  couplings to electrons,  $C_{e,V}^2 + C_{e,A}^2$ , via  $e^- + Z \rightarrow e^- + Z + Z'[\rightarrow e^+e^-]$  (where  $Z$  now represents the nucleus), and neutrino scattering from the TEXONO experiment [52]. We have also applied additional experimental limits on parity-violating Moller scattering [106, 107] and atomic parity violation [108, 109] as  $|C_{e,V} \times C_{e,A}| \leq 10^{-8}$  and  $|C_{e,A}| \left| \frac{188}{399} C_{u,V} + \frac{211}{399} C_{d,V} \right| \leq 1.8 \times 10^{-12}$ , respectively. In addition to the aforementioned constraints, IceCube NSI constraints [54] on  $Z'$  couplings have been applied. The full experimental constraints are summarised in Tab. 2.

### 3 The experimental framework sensitive to the $X_{17}$

In order to analyse the CE $\nu$ NS data from reactors we need to calculate the nuclear recoil spectrum in the SM as well as when including an extra vector boson exchange such as the  $X_{17}$ . Following the same general framework as in [57], with  $y = E_r/E_r^{\text{max}}$  being the fractional nuclear recoil energy and  $x = E_\nu/E_\nu^{\text{max}}$  being the fractional neutrino energy, we write the theoretical recoil spectrum as

$$\frac{dN_r}{dy} = \frac{m_{\text{det}} t_{\text{exp}} N_A}{M_A} \int_{\sqrt{y}}^1 \frac{d\sigma^{\nu_e N}}{dy} \frac{d\Phi_{\bar{\nu}_e}}{dx} dx, \quad (3.26)$$

where  $m_{\text{det}}$  is the mass of the detector,  $t_{\text{exp}}$  is the exposure time,  $M_A$  is the mass of the detector nucleus (in kg/kmol),  $N_A$  is the Avogadro's number,  $\frac{d\sigma^{\nu_e N}}{dy}$  is the differential cross-section for coherent elastic  $\nu_e N$ -scattering and  $\frac{d\Phi_{\bar{\nu}_e}}{dx}$  is the neutrino flux from a reactor. In order to have the same formalism for neutrinos from reactors and  $\pi^+$  decays at rest, we use  $E_\nu^{\text{max}} = m_\mu/2$  and  $E_r^{\text{max}} = m_\mu^2/(2M)$ . For a Germanium detector, as used both by the CONUS+ and Dresden-II experiments, with  $M = 67.6$  GeV it then follows that  $E_r^{\text{max}} = 82.5$  keV.

Using the same formalism as in [57], the CE $\nu$ NS cross-section including an additional  $Z'$  boson

with mass  $m_{Z'}$  for electron or muon neutrinos, can be written as

$$\frac{d\sigma^{\nu_{e/\mu}N}}{dy} = \frac{[N - (1 - 4 \sin^2 \theta_W)Z]^2 [F_V(y)]^2}{4\pi m_\mu^2} \left(1 - \frac{y}{x^2}\right) \left(\frac{G_F m_\mu^2}{\sqrt{2}} - \frac{C_{\text{eff}}^{\nu_{e/\mu}}}{y + m_{Z'}^2/m_\mu^2}\right)^2 \quad (3.27)$$

with the effective  $\nu_{e/\mu}N$  coupling  $C_{\text{eff}}^{\nu_{e/\mu}}$  mediated by the  $Z'$  given by the vector couplings of the  $Z'$  to the neutrinos ( $C_{\nu_{e/\mu},V}$ ) and quarks ( $C_{d/u,V}$ ) as

$$C_{\text{eff}}^{\nu_{e/\mu}} = \frac{C_{\nu_{e/\mu},V}[(N + 2Z)C_{u,V} + (2N + Z)C_{d,V}]}{N - (1 - 4 \sin^2 \theta_W)Z} \quad (3.28)$$

and  $F_V(y)$  being the form factor for which we use the Klein-Nystrand one [110],

$$F_V(y) = \frac{3 j_1(\sqrt{y}m_\mu R_A)}{\sqrt{y}m_\mu R_A} \frac{1}{1 + a^2 y m_\mu^2}, \quad (3.29)$$

where  $j_1$  is a spherical Bessel function of the first kind, i.e.,  $j_1(z) = (\sin z - z \cos z)/z^2$ ,  $R_A = 1.2A^{1/3}$  fm,  $A = 72.6$  and  $a = 0.7$  fm.

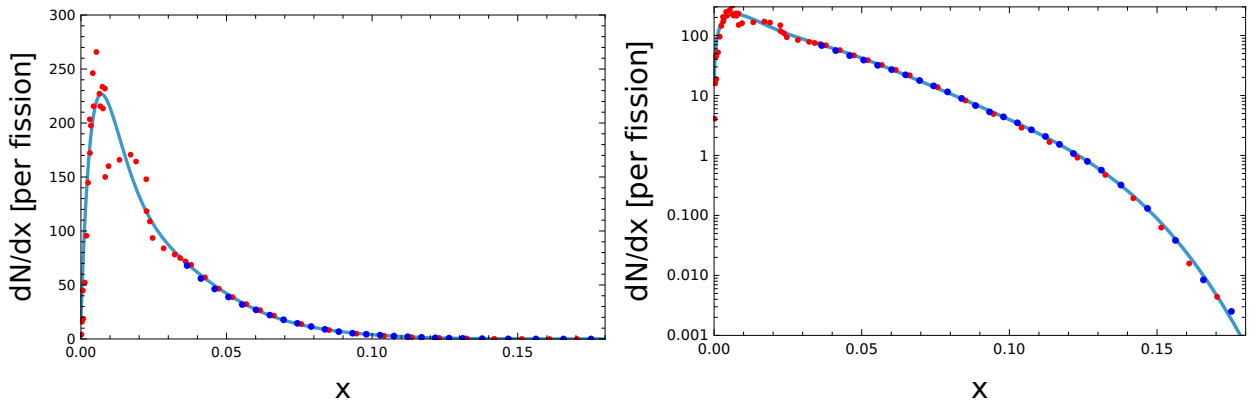


Figure 1: Neutrino spectra from fission reactors as calculated by Kopeikin (in red dots) together with data from Daya Bay (in blue dots) and fit used (solid line). The spectra are normalised per fission.

The reactor neutrino spectra have been calculated by Kopeikin [111] as well as by Mueller *et al.* [112] and Huber [113]. In the following we will also be using the Daya Bay measurement at high energies [114, 115]. As a first step towards modelling the neutrino flux we parametrise the latter per fission from a reactor as

$$\frac{dN_{\bar{\nu}_e}}{dx} = e^{a_1 + b_1 x + c_1 x^2 + d_1 x^3 + e_1 x^4 + f_1 x^5} + x e^{a_2 + b_2 x + c_2 x^2}, \quad (3.30)$$

where  $a_1 = 2.87593$ ,  $b_1 = 186.145$ ,  $c_1 = -3358.36$ ,  $d_1 = 31940.8$ ,  $e_1 = -139054$ ,  $f_1 = 193450$ ,  $a_2 = 11.2864$ ,  $b_2 = -149.915$  and  $c_2 = -452.33$ . The parameters have been obtained by fitting to the Daya Bay data for  $x > 0.0379$  ( $E_\nu > 2$  MeV) and then subsequently to the calculation by Kopeikin. The resulting fit is also shown in Fig. 1 together with the data used.

The neutrino flux from a given reactor is then obtained as

$$\frac{d\Phi_{\bar{\nu}_e}}{dx} = \frac{\Phi}{N_{\bar{\nu}_e}} \frac{dN_{\bar{\nu}_e}}{dx}, \quad (3.31)$$

where the total fluxes for the Dresden-II and CONUS+ experiments are:

- $\Phi_{\text{Dresden-II}} = 4.8 \times 10^{13} \text{ cm}^2/\text{s}$  [2],
- $\Phi_{\text{CONUS+}} = 1.5 \times 10^{13} \text{ cm}^2/\text{s}$  [3],

with the number of neutrinos per fission  $N_{\bar{\nu}_e} = 6.8$ , from the parametrisation in agreement with [111]. For reference, the resulting recoil spectrum in the SM is shown in Fig. 2. From the figure it is clear that the spectrum resulting from reactor neutrinos is very steeply falling compared to the one from  $\pi^+$  decays at rest.

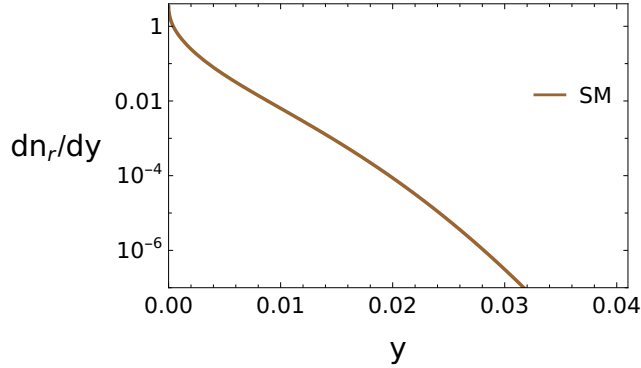


Figure 2: Nuclear recoil spectrum in the SM from reactor neutrinos and assuming a Germanium detector before smearing and quenching. Arbitrary normalisation.

Note that a given nuclear recoil energy requires a minimum neutrino energy which is reflected by the constraint  $x > \sqrt{y}$  in Eq. (3.26). For example, neutrinos with at least 2 MeV ( $x = 0.0379$ ) are needed to contribute to the recoil spectrum at  $E_r = 0.118 \text{ keV}$  ( $y = 0.0014$ ) for a Germanium detector. Therefore, the modelling of the shape of the neutrino energy spectrum at small  $x$  is not so important, as long as the total number of neutrinos per fission is correct, since the shape of the spectrum in this region is determined by the energy resolution of the detector (as it will become clear below).

From the theoretical recoil spectrum in Eq. (3.26), the experimentally observed one is obtained by taking into account the Quenching Factor (QF), which describes the conversion of the nuclear recoil energy to an ionisation signal, as well as the finite detector resolution giving

$$\frac{dN_r}{dy_{\text{rec}}} = \int_{y_{\text{min}}}^1 R(y_{\text{rec}}, y_{\text{ion}}) \frac{dN_r}{dy} dy, \quad (3.32)$$

where  $y_{\text{rec}}$  is the reconstructed energy fraction,  $y_{\text{ion}}$  is the fractional ionisation energy ( $y_{\text{ion}} = E_{\text{ion}}/E_r^{\text{max}}$ ) and  $R(y_{\text{rec}}, y_{\text{ion}})$  describes the detector response in terms of the resolution, which we define below. The lower integration limit,  $y_{\text{min}} = \frac{\eta}{E_r^{\text{max}}} \frac{1}{Q(y_{\text{min}})}$ , is the minimal fractional ionisation energy in terms of the minimal ionisation energy  $\eta = 2.96 \text{ eV}_{\text{ee}}$  needed to create an electron-hole pair in Germanium and  $Q(y)$  is the QF.

In the following we will mainly be using the Lindhard model to describe the quenching. In this model the fractional ionisation energy created by the nuclear recoil is written as

$$y_{\text{ion}} = Q(y)y, \quad (3.33)$$

where

$$Q_{\text{Lindhard}}(y) = \frac{kg(y)}{1 + kg(y)} \quad (3.34)$$

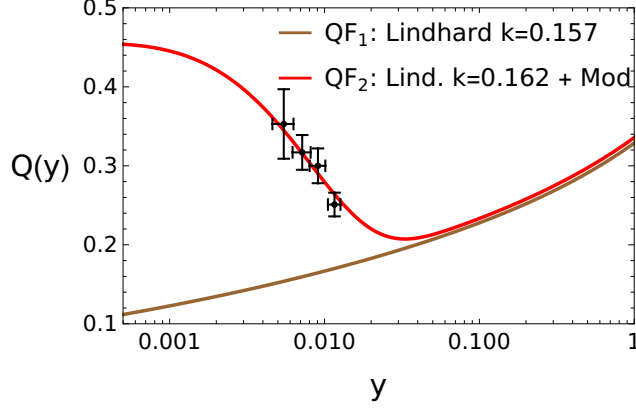


Figure 3: QFs used:  $QF_1$  is the Lindhard model with  $k = 0.157$  and  $QF_2$  is the Lindhard model with  $k = 0.162$  and a modification added to describe the data points.

and  $g(y) = 3(C_Z y)^{0.15} + 0.7(C_Z y)^{0.60} + C_Z y$  with  $C_Z = E_r^{\max} \times 11.5/Z^{7/3}$  and  $k = 0.157$ . The resulting QF is shown in Fig. 3 together with a modified QF which has been constructed to describe data from [116] which are also shown in the figure.

To describe these data we simply add the modification

$$Q_{\text{Mod}}(y) = 0.36 \exp(-120y) \quad (3.35)$$

to the QF. In addition, in order to illustrate the uncertainties related to the QF we also modify the factor  $k$  to 0.162. Thus we will consider the two following QFs

$$QF_1 = Q_{\text{Lindhard}}(k = 0.157), \quad (3.36)$$

$$QF_2 = Q_{\text{Lindhard}}(k = 0.162) + Q_{\text{Mod}}. \quad (3.37)$$

With the two QFs defined, we then also get the corresponding minimal fractional recoil energies in Eq. (3.32). For the Lindhard model  $QF_1$  this becomes  $y_{\min} = 0.00034$  whereas for the modified Lindhard model  $QF_2$  it is given by  $y_{\min} = 0.000083$

Next we consider the effects of the finite detector resolution as described by

$$R(y_{\text{rec}}, y_{\text{ion}}) = \frac{2}{1 + \text{Erf}\left(\frac{y_{\text{ion}}}{\sqrt{2}\sigma}\right)} \frac{1}{\sqrt{2\pi}\sigma} \exp\left[-\frac{(y_{\text{rec}} - y_{\text{ion}})^2}{2\sigma^2}\right]. \quad (3.38)$$

where  $\sigma = \sigma_E/E_r^{\max}$  is a dimensionless width with

$$\sigma_E^2 = \sigma_n^2 + E_{\text{ion}}\eta F, \quad (3.39)$$

where  $\eta = 2.96 \text{ eV}_{ee}$ , the Fano factor  $F = 0.11$  and  $\sigma_n$  is the intrinsic resolution of the detector for which we use

$$\sigma_n^{\text{Dresden-II}} = 68.5 \text{ eV}_{ee}, \quad (3.40)$$

$$\sigma_n^{\text{CONUS+}} = 20.0 \text{ eV}_{ee}. \quad (3.41)$$

Note that the transformation above from  $\frac{dN_r}{dy}$  to  $\frac{dN_r}{dy_{\text{rec}}}$  preserves the total number of events if the resolution  $\sigma$  is changed, as long as  $y_{\min}$  is kept constant and the factor  $2/(1 + \text{Erf}(\frac{y_{\text{ion}}}{\sqrt{2}\sigma}))$ , which compensates for the Gaussian distribution being cut off, is included. In other words:

$$\int_0^1 \frac{dN_r}{dy_{\text{rec}}} dy_{\text{rec}} = \int_0^1 \int_{y_{\min}}^1 R(y_{\text{rec}}, Q(y)y) \frac{dN_r}{dy} dy dy_{\text{rec}} = \int_{y_{\min}}^1 \frac{dN_r}{dy} dy. \quad (3.42)$$

However, since  $y_{\min}$  depends on the QF, the total number of events will change if the QF is changed in such a way that  $y_{\min}$  changes.

The resulting detector signals for the Dresden-II and CONUS+ experiments are shown in Fig. 4. Comparing to Fig. 2, there are two main effects on the spectrum: (i) the quenching pushes the spectrum to much smaller fractional recoil energies and (ii) the finite detector resolution gives a substantial smearing of the spectrum - especially for the Dresden-II experiment - and in addition has a large impact on the normalisation in the region  $y_{\text{rec}} \gtrsim 0.002$  corresponding to  $E_{\text{ion}} \gtrsim 165 \text{ eV}_{\text{ee}}$ . It is also clear that using different QFs has a very large impact on the spectral shape as well as normalisation. We finally note that a larger smearing gives higher sensitivity to smaller recoil energies.

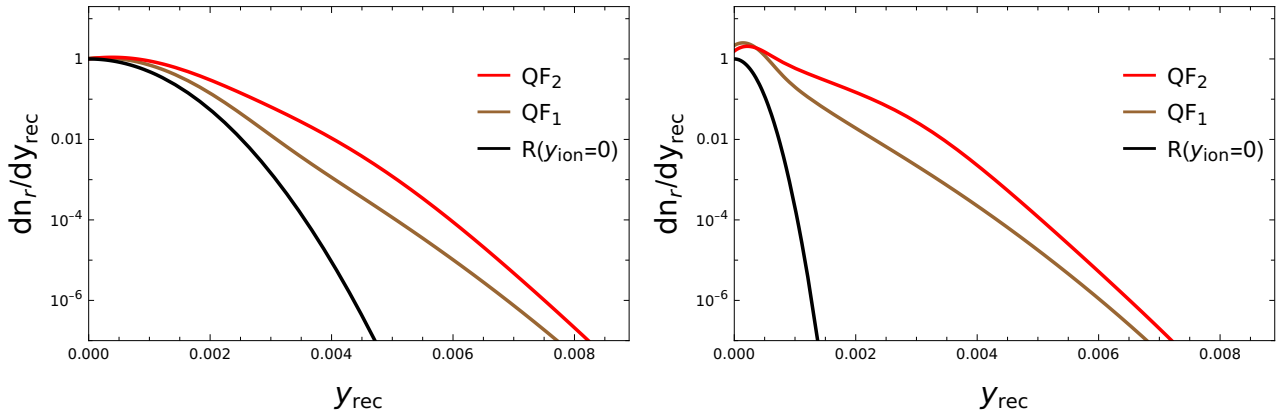


Figure 4: Shape of nuclear recoil spectra for Dresden-II (left) and CONUS+ (right) after smearing and quenching with different QFs as well as the inherent resolution of the detector given by  $R(y_{\text{rec}}, 0)$  normalised such that  $R(0, 0) = 1$ .

In order to quantify the uncertainty from quenching, we define the QF uncertainty by calculating the ratio

$$R_{\text{QF}} = \left| \frac{\left. \frac{dN_r}{dy_{\text{rec}}} \right|_{\text{QF2}} - \left. \frac{dN_r}{dy_{\text{rec}}} \right|_{\text{QF1}}}{\left. \frac{dN_r}{dy_{\text{rec}}} \right|_{\text{QF1}}} \right|. \quad (3.43)$$

As can be seen in Fig. 5, the uncertainty defined in this way reaches about a factor 10 as its maximal value in the region where there are experimental data from reactors. In addition, the peak uncertainty is obtained for quite different values of the detector signal, as it depends on the intrinsic resolution of the detector. For comparison, the figure also shows the same uncertainty calculated for  $\pi^+$  decay at rest, showing that in this case the uncertainty is more than an order of magnitude smaller above the detector threshold of about  $y_{\text{rec}} \approx 0.002$  ( $E_{\text{rec}} \approx 160 \text{ eV}_{\text{ee}}$ ).

To convert the calculations done so far to event counts, that can be compared to experiment, we need the detector masses and exposure time. For CONUS+ they have a detector mass of 2.83 kg and a corresponding exposure of 115.5 days giving a total of 327 kg days whereas for Dresden-II the mass is 2.924 kg and the exposure 96.4 days giving 282 kg days.

With the above we get the predicted number of nuclear recoil events for CONUS+ in the SM (integrating from  $y_{\text{rec}} = 0.160/82.5$  to  $y_{\text{rec}} = 0.400/82.5$ ) to be 381 with  $\text{QF}_1$  and 3622 with  $\text{QF}_2$  which should be compared to the collaborations calculation of  $347 \pm 59$  and the observation of  $395 \pm 106$  whereas for the Dresden-II experiment we get (integrating from  $y_{\text{rec}} = 0.200/82.5$

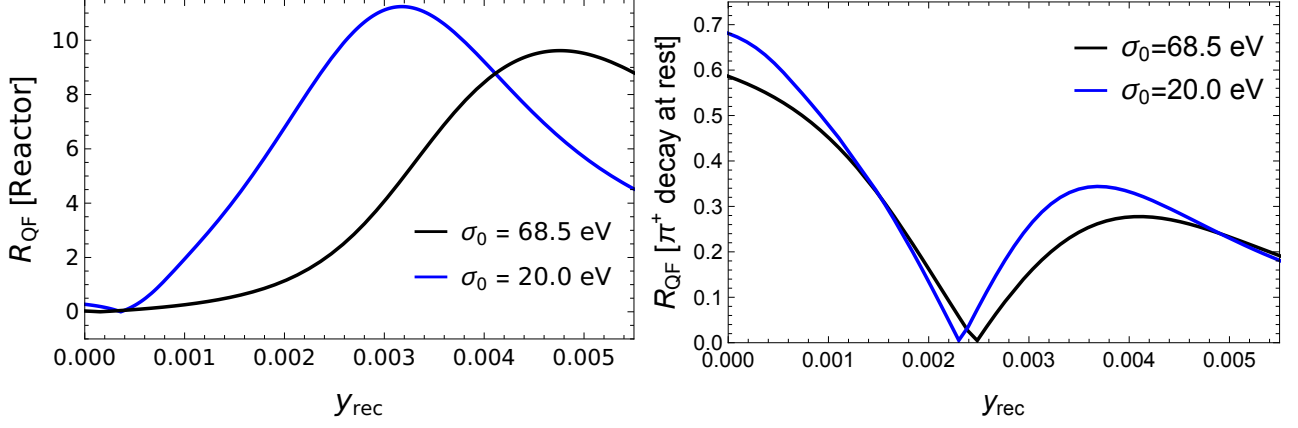


Figure 5: QF uncertainty for reactor (left) and  $\pi^+$  decay at rest (right) neutrinos with the same detector resolution as Dresden-II (black) and CONUS+ (blue).

to  $y_{\text{rec}} = 0.400/82.5$ ) 2245 nuclear recoil events with QF<sub>1</sub> and 9817 with QF<sub>2</sub>. Note that even though the detector masses and exposure times are quite similar, the CONUS+ sees much fewer events due to the flux being a factor three smaller and the resolution being higher.

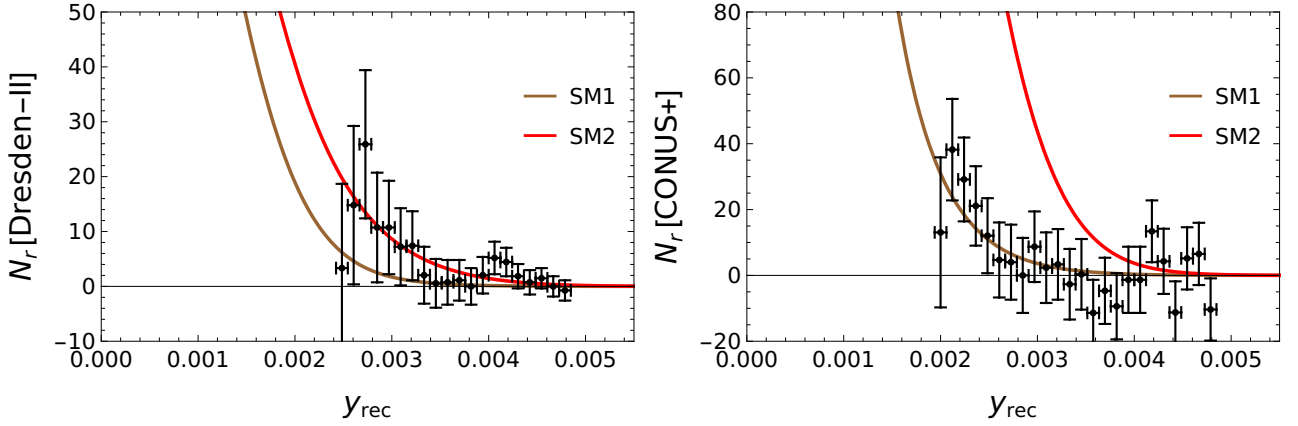


Figure 6: Nuclear recoil spectra after smearing and quenching compared to data as published using the QF<sub>1</sub> or QF<sub>2</sub> in the SM. The data has been normalised in the same way as done by the respective experiments.

Looking instead at the detected recoil spectra, as shown in Fig. 6, we see that the CONUS+ data are in very good agreement with the SM when using QF<sub>1</sub> but not at all with QF<sub>2</sub> whereas the Dresden-II data seems to be in much better agreement with the SM when using QF<sub>2</sub>. It has recently been pointed out [78] that no QF can be found making the two datasets agree with each other. In the following we will on the one hand show that the datasets can be made to agree with each other in the SM by including the QF uncertainty as defined in Eq. (3.43). More interestingly, we will also show that the datasets can be made to agree with each other using the standard Lindhard model and adding the  $X_{17}$  with appropriate couplings.

### 3.1 Statistical and systematic errors

In order to quantify these statements in more detail we will use the following  $\chi^2$  function to analyse the statistical significance of the data:

$$\chi^2 = \sum_i \left( \frac{(1 + \rho)x_i - \mu_i}{\sigma_i} \right)^2 + \left( \frac{\rho}{\sigma_{\text{sys}}} \right)^2, \quad (3.44)$$

where  $x_i$  are the model predictions for the number of events in a bin and  $\mu_i$  are the number of observed events with  $\sigma_i$  being the corresponding errors. In addition,  $\rho$  is an overall scale factor, with an overall systematic uncertainty  $\sigma_{\text{sys}}$ . The scale factor is determined by minimising the  $\chi^2$  with respect to  $\rho$  giving

$$\rho = \frac{\sum_i \frac{x_i(\mu_i - x_i)}{\sigma_i^2}}{\frac{1}{\sigma_{\text{sys}}^2} + \sum_i \frac{x_i^2}{\sigma_i^2}}. \quad (3.45)$$

Any systematic uncertainties which vary from bin to bin,  $\sigma_{\text{sys},i}$ , are included in the errors  $\sigma_i$  using  $\sigma_i^2 = \sigma_{\text{stat},i}^2 + \sigma_{\text{sys},i}^2 x_i^2$ , which corresponds to including a scale factor  $\rho_i$  for each bin where, in addition, we use the SM values for  $x_i$  for simplicity. To be more clear, when including the QF uncertainty from Eq. (3.43), we will calculate the average  $R_{\text{QF},i}$  for each bin and then add them quadratically to the errors reported by the experiments setting  $\sigma_{\text{sys},i} = R_{\text{QF},i}$ .

When analysing the reactor datasets, we will for definiteness use the same scale uncertainties for both of them:  $\sigma_{\text{sys}} = 0.15$  when the QF uncertainty is handled separately for each bin and  $\sigma_{\text{sys}} = 0.17$  when it is included as part of the overall uncertainty following [3].

With  $\chi^2$  defined as in Eq. (3.44) we get  $\chi^2 = 11.6$  (37.4) for CONUS+ with QF<sub>1</sub>(QF<sub>2</sub>) and  $\chi^2 = 14.4$  (8.2) for Dresden-II with QF<sub>1</sub>(QF<sub>2</sub>) in the SM when not taking into account the QF uncertainty bin-by-bin. Adding the latter, the  $\chi^2$  values change to  $\chi^2 = 7.2$  for CONUS+ and  $\chi^2 = 10.9$  for Dresden-II, in both cases with QF<sub>1</sub>. Comparing these  $\chi^2$  values with the number of data points used in the calculation, 24 for CONUS+ and 20 for Dresden-II, we see that the  $\chi^2$  per degree of freedom is well below one except when using QF<sub>2</sub> for the CONUS+ data and not including the QF uncertainty. Based on these observations, we will use QF<sub>1</sub>, with or without the QF uncertainty, as the main model for analysing the data.

More interestingly, it is also possible to explain the apparent differences between the CONUS+ and Dresden-II experiments by an additional light  $Z'$  as defined by the cross-section in Eq. (3.27). A priori, such an additional light  $Z'$  could have any mass and effective coupling to nuclei and we have therefore calculated the  $\chi^2$  when varying these two parameters to see what ranges are preferred/allowed by the reactor data. The results are shown in Fig. 7. From the figure, it is clear that with the QF uncertainty added there is a range of allowed  $C_{\text{eff}}^{\nu_e}$  values for any given  $m_{Z'}$ . For larger masses the limits scale as  $C_{\text{eff}}^{\nu_e}/m_{Z'}^2$ , as is evident from Eq. (3.27). At the same time, when the QF uncertainty is not added, there is a preferred region  $m_{Z'} \approx [13, 25]$  MeV and  $C_{\text{eff}}^{\nu_e} \approx [0.5, 1.5] \cdot 10^{-8}$  which has  $\chi^2 \approx 24$  compared to the SM value 26. More specifically, for  $m_{Z'} = 16.7$  MeV, the  $\chi^2$  for different effective neutrino nucleus couplings is shown in Fig. 8. Here it is clear that the data are better described by including a 16.7 MeV  $Z'$  with  $C_{\text{eff}}^{\nu_e}$  being either slightly negative or close to  $[0.7, 0.9] \cdot 10^{-8}$  irrespectively of whether the QF uncertainty is taken into account or not.

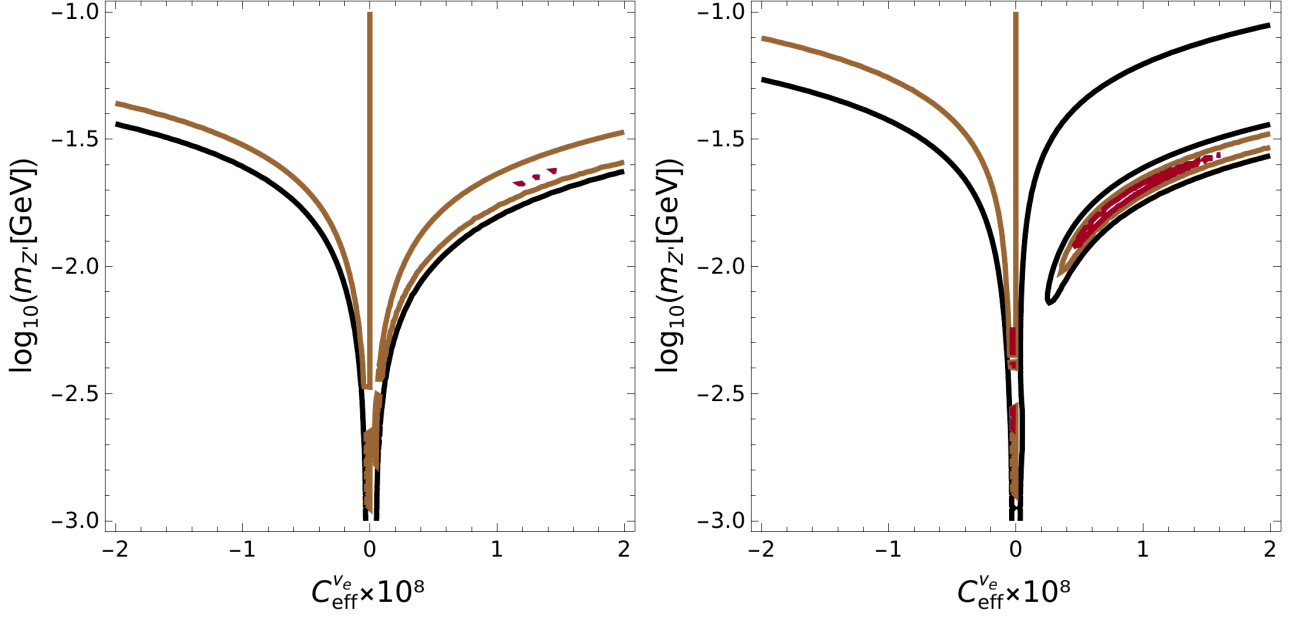


Figure 7: The  $\chi^2$  contours for combined reactor datasets with (left) and without (right) bin-by-bin QF uncertainty added to data. Brown = SM, Black = SM+6, Red = SM-2.

### 3.2 Combining reactor and spallation source datasets

Before comparing the reactor datasets to a specific  $X_{17}$  model, we also want to include other data on CE $\nu$ NS from the COHERENT experiment. We will be using both the Argon [59] and Caesium Iodine [61] data as well as the recent Germanium data [63].

We will use the same framework for analysing these data as the reactor ones, although generalised to include also muon neutrinos. In short, the cross-section for  $\nu_{e/\mu}$  nucleus scattering is given by Eq. (3.27) and the neutrino fluxes from the  $\pi^+$  decay at rest are

$$\frac{d\Phi_{\nu_e}}{dx} = \frac{rN_{\text{POT}}}{4\pi L^2} 12x^2(1-x), \quad (3.46)$$

$$\frac{d\Phi_{\bar{\nu}_\mu}}{dx} = \frac{rN_{\text{POT}}}{4\pi L^2} 2x^2(3-2x), \quad (3.47)$$

$$\frac{d\Phi_{\nu_\mu}}{dx} = \frac{rN_{\text{POT}}}{4\pi L^2} \delta(x-x_0), \quad (3.48)$$

where  $r$  is the number of  $\pi^+$  produced per proton,  $N_{\text{POT}}$  is the number of protons on target,  $L$  is the distance travelled by the neutrinos and

$$x_0 = \frac{m_{\pi^+}^2 - m_\mu^2}{m_\mu m_{\pi^+}} \approx 0.564 \quad (3.49)$$

is the scaled energy of the muon neutrinos from the two-body decay. Convoluting the cross-section with the neutrino fluxes, the theoretical nuclear recoil spectrum for neutrinos from pion decays at rest is then given by

$$\frac{dN_r}{dy} = \frac{rN_{\text{POT}}}{4\pi L^2} \frac{1}{2\pi m_\mu^2} [N - (1 - 4\sin^2\theta_W)Z]^2 \frac{m_{\text{det}}}{M_A} N_A [F_V(y)]^2 \quad (3.50)$$

$$\left\{ \left( \frac{G_F m_\mu^2}{\sqrt{2}} - \frac{C_{\text{eff}}^{\nu_e}}{y + m_{Z'}/m_\mu^2} \right)^2 \frac{dn_{\nu_e}}{dy} + \left( \frac{G_F m_\mu^2}{\sqrt{2}} - \frac{C_{\text{eff}}^{\nu_\mu}}{y + m_{Z'}/m_\mu^2} \right)^2 \frac{dn_{\nu_\mu}}{dy} \right\},$$

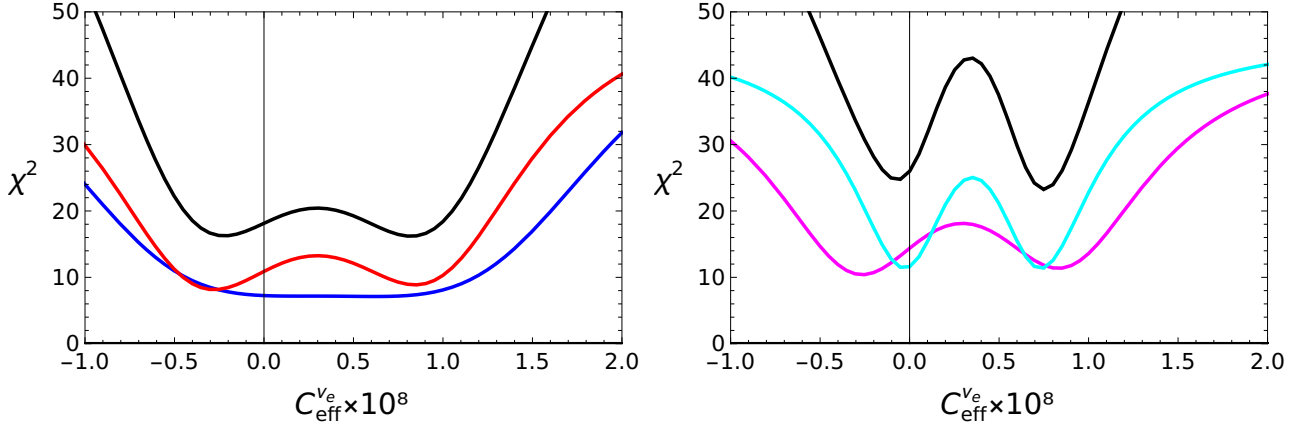


Figure 8: The  $\chi^2$  for the individual (magenta, red = Dresden-II and cyan, blue = CONUS+) as well as combined (black) reactor datasets: with (left) and without (right) QF uncertainty added to data for  $m_{Z'}$  = 16.7 MeV.

where

$$\frac{dn_{\nu_e}}{dy} = \frac{1}{2} - 3y + 4y^{3/2} - \frac{3}{2}y^2, \quad (3.51)$$

$$\frac{dn_{\nu_\mu}}{dy} = \frac{1}{2} - 2y + 2y^{3/2} - \frac{1}{2}y^2 + \left(\frac{1}{2} - \frac{y}{2x_0^2}\right) \Theta\left(1 - \frac{y}{x_0^2}\right). \quad (3.52)$$

(For more details we refer to [57].)

To analyse the COHERENT data we use the experimental conditions as published by the collaboration and summarised in appendix A. Similarly to when analysing the reactor data, we use  $\text{QF}_1$  for Germanium data. However, the QF uncertainty is only considered for the reactor datasets. Thus, the systematic scale uncertainties in the different COHERENT datasets are as follows:  $\sigma_{\text{sys}}^{\text{Ar}} = 0.13$  (Argon),  $\sigma_{\text{sys}}^{\text{CsI}} = 0.12$  (Caesium Iodine),  $\sigma_{\text{sys}}^{\text{Ge}} = 0.103$  (Germanium).

The effective neutrino nucleus couplings, given by Eq. (3.28), include a dependence on the number of neutrons and protons. The main effect is that the  $C_{d,V}$  coupling carries a  $\sim 10\%$  larger weight than  $C_{u,V}$  from  $N$  being larger than  $Z$  for the nuclei of interest. In detail, this dependence varies from nucleus to nucleus. In order to be able to only use two effective neutrino nucleus couplings we approximate this dependence by using  $C_{\text{eff}}^{\nu_e/\mu}(\text{Ar}) = 1.020 C_{\text{eff}}^{\nu_e/\mu}(\text{Ge})$  and  $C_{\text{eff}}^{\nu_e/\mu}(\text{CsI}) = 0.953 C_{\text{eff}}^{\nu_e/\mu}(\text{Ge})$ , which are obtained by taking the average of the nuclear dependence of the effective neutrino quark couplings defined analogously to Eq. (3.28).

With these definitions, we can now calculate the experimentally observed recoil spectra also for the COHERENT data sets and compare to the published data using the  $\chi^2$  function defined by Eq. (3.44). The resulting  $\chi^2$  for  $m_{Z'} = 16.7$  MeV and as a function of the effective neutrino nucleus couplings -  $C_{\text{eff}}^{\nu_e}$  and  $C_{\text{eff}}^{\nu_\mu}$  - is shown in Fig. 9. As can be seen from the figure, adding the COHERENT data does not change the preferred regions for  $C_{\text{eff}}^{\nu_e}$ . At the same time, the COHERENT data constrains the  $C_{\text{eff}}^{\nu_\mu}$  coupling, although not quite as strongly as the reactor data constrain  $C_{\text{eff}}^{\nu_e}$ . It is also clear from the figure that the QF uncertainty does not have a big impact on the preferred regions even though the allowed regions are significantly larger when it is included.

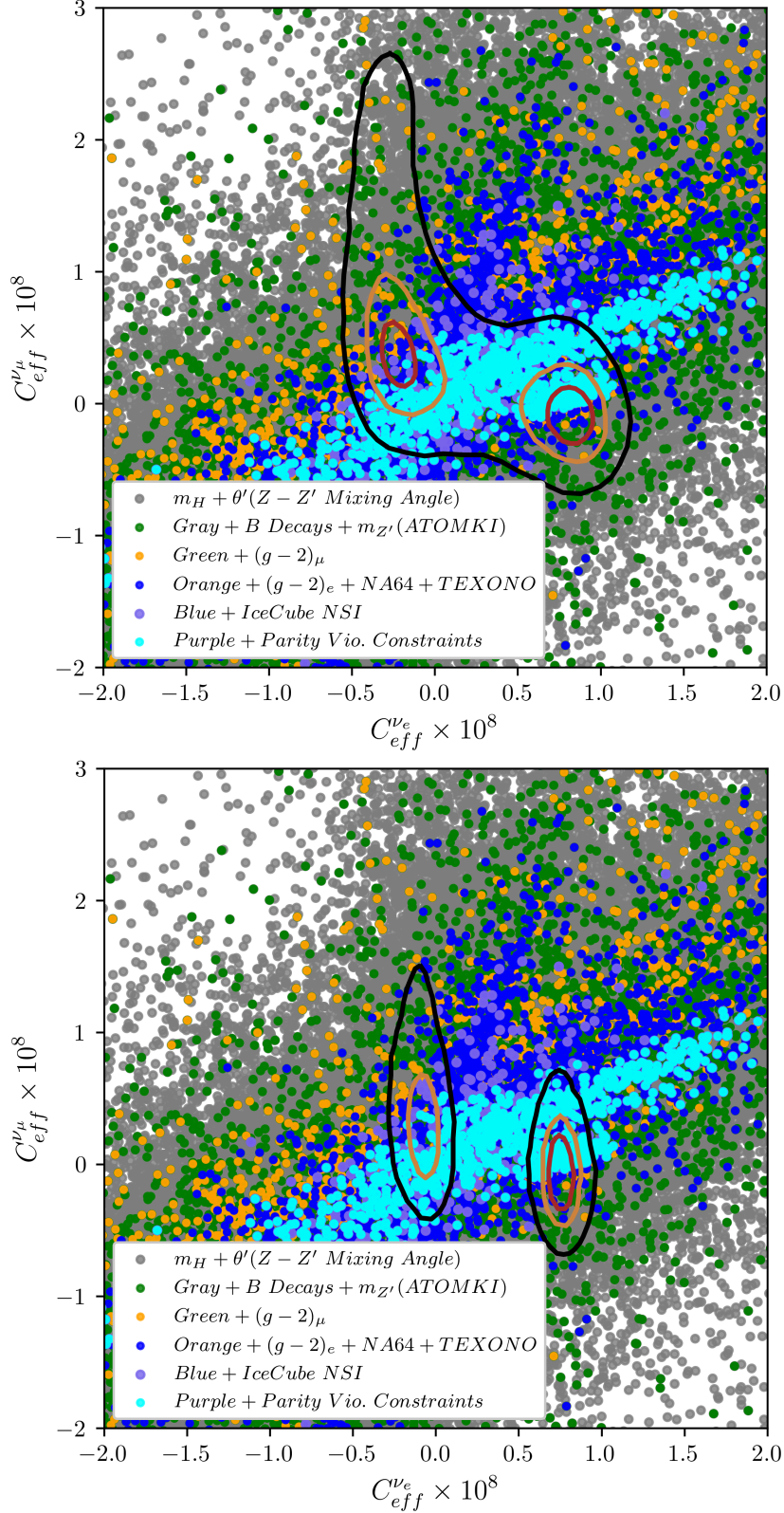


Figure 9: The  $\chi^2$  contours for combined reactor and COHERENT datasets with (upper) and without (lower) QF uncertainty added to reactor data for  $m_{Z'} = 16.7$  MeV. Brown = SM, Black = SM+6, Red = SM-2. The coloured points show the results of the scan over parameters of the  $X_{17}$  model considered as defined in Tab. 1 after applying various constraints as indicated in the caption and detailed in Tab. 2.

The figure also shows the points resulting from a scan over the parameters of the  $X_{17}$  model presented in section 2 and how they are constrained by the various experimental limits as collected in Tab. 2. As can be seen from the figure, the application of all constraints results in a rather narrow band of allowed effective neutrino nucleus couplings from other measurements. The CE $\nu$ NS constrains the parameters of the model even more - in particular when not including the quenching factor uncertainty.

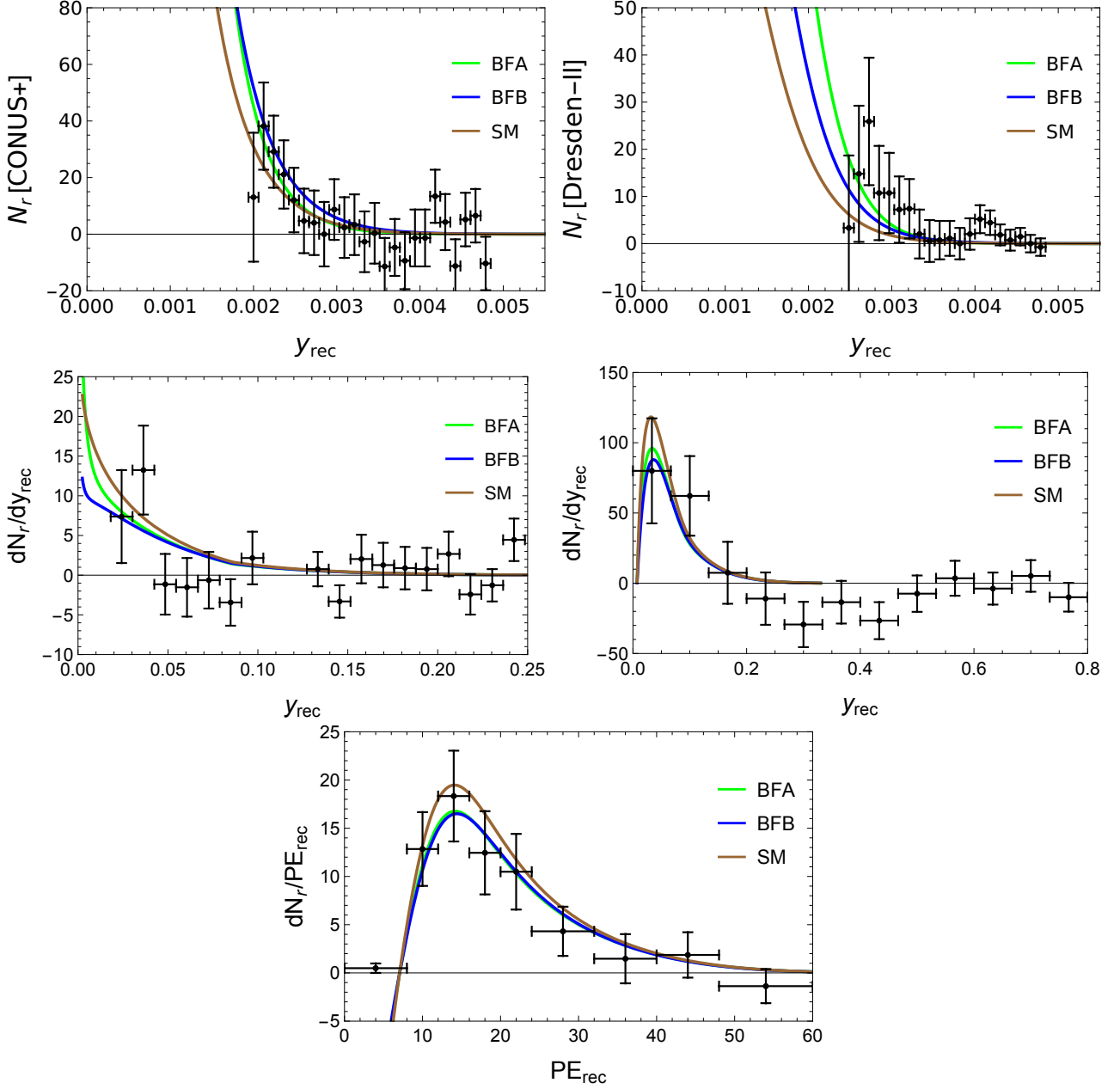


Figure 10: Nuclear recoil data from CONUS+ (upper left), Dresden-II (upper right), COHERENT Germanium (middle left), COHERENT Argon (middle right) and COHERENT CsI (lower) compared to the SM and best fit points A and B for  $m_{Z'} = 16.7$  MeV.

All in all, from Fig. 9 we identify two distinct best fit points (or regions),

$$\text{BFA: } C_{\text{eff}}^{\nu_e} = 0.75 \times 10^{-8}, \quad C_{\text{eff}}^{\nu_\mu} = -0.05 \times 10^{-8},$$

$$\text{BFB: } C_{\text{eff}}^{\nu_e} = -0.10 \times 10^{-8}, \quad C_{\text{eff}}^{\nu_\mu} = 0.35 \times 10^{-8},$$

that we analyse in some more detail below. First of all, in Fig. 10, we show the respective best fit points compared to the data used for the fit. As expected, both best fit points describe the data equally well. At the same time, it is clear that the spectra from the two fits differ at small nuclear recoils, below what has been measured by the COHERENT collaboration. Especially for the Argon and Caesium Iodine data, the detector efficiency cuts off the spectra for small recoil energies. For the reactor data, more data and a lowering of the detector threshold would be needed to be able to distinguish the two.

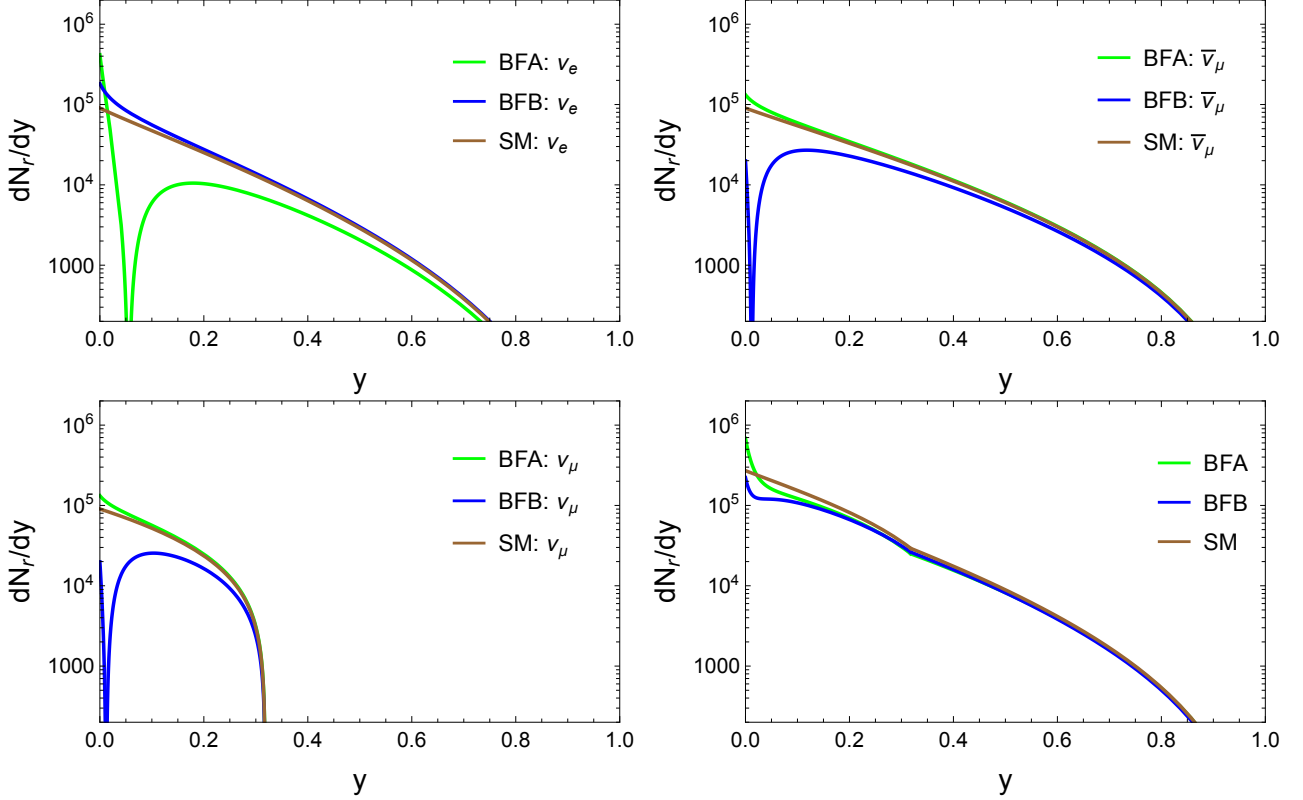


Figure 11: Theoretical recoil spectra for the best fit points A and B compared to SM for  $m_{Z'} = 16.7$  MeV and assuming a Germanium detector. Upper left (right) shows the  $\nu_e$  ( $\bar{\nu}_\mu$ ) induced contribution whereas the lower left (right) plot shows the  $\nu_\mu$  (sum of all) contribution(s).

To analyse in more detail the distinctions between the two best fit points, we show in Fig. 11 the theoretical recoil spectra for electron and (anti) muon neutrinos separately as well as the sum. From the figure it is clear that, in both BFA and BFB, the nuclear recoil spectrum for  $\nu_e$ -scattering is enhanced compared to the SM (upper left plot) at very small recoil energies,  $y \lesssim 0.02$  whereas, at larger recoil energies, the spectrum is enhanced in a similar way in BFB and heavily suppressed in BFA. There is even a point where the recoil spectrum in BFA vanishes due to negative interference between the  $X_{17}$  and the SM.

In order to fit the observations by COHERENT, this means that the  $\nu_\mu$  and  $\bar{\nu}_\mu$ -scattering (upper right and lower left plot respectively) induced recoil spectra at larger recoil energies,  $y \gtrsim 0.2$ , are enhanced in BFA and suppressed in BFB in such a way that the sum of all contributions (lower right plot) is the same. Thus, in order to separate the two scenarios, one needs to measure the recoil spectrum at lower energies than has been done at COHERENT: in other words, in the region  $0.02 \lesssim y \lesssim 0.2$ .

We then also note that, in principle, the timing information from SNS events could help to

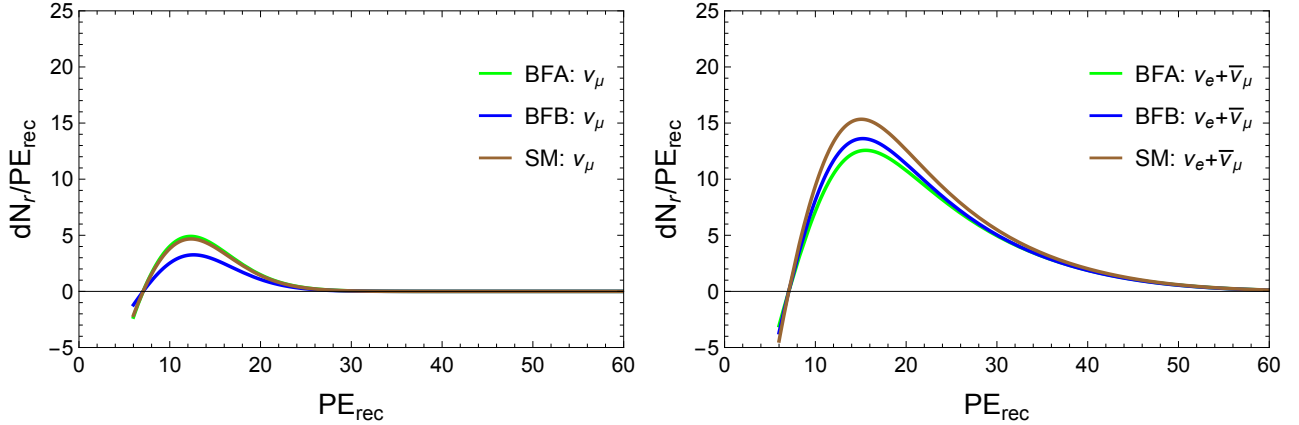


Figure 12: Recoil spectra after quenching and smearing for the best fit points A and B compared to SM for  $m_{Z'} = 16.7$  MeV and assuming a CsI detector with the same characteristics as the COHERENT one. Left (right) prompt (non-prompt) contributions assuming that the timing information could be used to separate the two completely.

distinguish the prompt  $\nu_{\mu}$  from the non-prompt  $\bar{\nu}_{\mu}$  and  $\nu_e$  where the latter two have higher energies, but not to separate  $\nu_e$  from  $\bar{\nu}_{\mu}$ . At the same time, as is clear from Fig. 12, even with a perfect separation between  $\nu_{\mu}$  on the one hand and  $\bar{\nu}_{\mu}$  and  $\nu_e$  on the other, the limited acceptance at small recoil energies for the present COHERENT data makes the differences between the two scenarios very small as exemplified by the CsI results in the plot. So in the end it will be necessary to go to lower recoil energies to make full use of the timing information.

## 4 Conclusions and outlook

By analysing nuclear recoil spectra arising from CE $\nu$ NS utilising electron anti-neutrinos from nuclear reactors and adding a light vector mediator in the form a  $Z'$  boson, we have shown that the data from the CONUS+ and Dresden-II experiments point to a preferred mass region (around 16.7 MeV) close to that of the  $X_{17}$ , which has emerged as a possible explanation of the ATOMKI anomaly. In fact, including the  $X_{17}$  also makes it possible to resolve the tension between the CONUS+ and Dresden-II data. The difference in the observations between the two experiments is then to a large extent explained by the differences in detector resolution which gives a different sensitivity to the  $X_{17}$ .

Assuming that, indeed, it is the  $X_{17}$  that explains this tension between the two experiments, we also find that the preferred effective coupling between the electron anti-neutrinos and nuclei mediated by the  $X_{17}$  is positive, in contrast to what is the case in the  $B-L$  model and variations thereof. As such, this positive coupling is more in line with what is observed in the so-called universal models, which however do not fulfil the anomaly conditions.

In addition to the data from the two reactor experiments, which have observed CE $\nu$ NS, we also add available data from the COHERENT experiment. When combined with the reactor data, these data also constrain the effective couplings between muon (anti-)neutrinos and nuclei mediated by the  $X_{17}$ . By making a combined fit to the data, we identified two regions of preferred effective neutrino-nucleus couplings for the  $X_{17}$  that are able to describe all available CE $\nu$ NS data from observations.

From the analysis of the data it is also clear that models with non-universal flavour couplings are preferred. In fact, the preferred regions would not have been seen in a model with flavour universal couplings. Our analysis also shows that although currently the uncertainties from the quenching factor of Germanium is very large, the preferred regions of the effective neutrino-nucleus couplings mediated from the  $X_{17}$  are more or less the same even irrespective of whether this uncertainty is included or not. In the end, using a minimal anomaly-free model to add the  $X_{17}$  to the SM, we found that such a setup is indeed able to describe the  $CE\nu NS$  data at the same time as it fulfils all the currently known constraints from other precision measurements.

Going forward, our analysis also shows the importance of lowering the detector thresholds for experiments at spallation sources, but still being in the region with larger nuclear recoils than what can be detected with reactor neutrinos, where we expect larger differences between the SM and models with a  $X_{17}$ . We have also shown that adding timing information to distinguish prompt neutrinos from the  $\pi^+$  decays and delayed ones from the  $\mu^+$  decays could reveal dips in the recoil spectrum arising from negative interference between the  $Z$  boson of the SM and the  $X_{17}$ .

Finally, we note that there is a strong need to understand the quenching factors for Germanium detectors better in order to make full use of the  $CE\nu NS$  data, in particular from reactors, for constraining BSM physics, such as the intriguing  $X_{17}$ .

## Note added

Shortly after finishing this paper, new results on the measurement of  $CE\nu NS$  on a Germanium target by the COHERENT collaboration appeared [117]. According to the collaboration, these data are more in line with the SM expectations. Such a change would have only a minor impact on our analysis, possibly resulting in a slight change of the preferred value of the effective muon-neutrino nucleus coupling.

## Acknowledgments

SM is supported in part through the NExT Institute and STFC Consolidated Grant ST/X000583/1. The work of YH is supported by the Balikesir University Scientific Research Projects via the Grant No. BAP-2022/083. YH thanks SM and Rikard Enberg for their hospitality during a visit to Uppsala, where part of this work was carried out under the auspices of the Short Term Scientific Mission (STSM) via the COST Action CA21106 ‘‘COSMIC WISPer’’.

## A Detector performance for COHERENT data

In this appendix, based on the original publications [59–62], we give a short summary of the assumptions regarding the detector performance that has been made when analysing the COHERENT data.

## A.1 Argon

We use  $N_{\text{POT}} = 1.38 \times 10^{23}$ ,  $r = 0.09$ ,  $L=27.5$  m,  $N = 21.95$ ,  $Z = 18$ , and  $m_{\text{det}} = 24.4$  kg. The QF is given by

$$\text{QF}_{\text{Ar}} = 0.24 + 0.00078 y E_{\text{max}}^{\text{Ar}} \quad (\text{A.53})$$

where  $E_{\text{max}}^{\text{Ar}} = 150$  is given in keV. The fractional ionisation energy is thus given by,

$$y_{\text{ion}}^{\text{Ar}} = \text{QF}_{\text{Ar}} y. \quad (\text{A.54})$$

The energy resolution is in turn given by

$$R_{\text{Ar}}(y_{\text{rec}}^{\text{Ar}}, y_{\text{ion}}^{\text{Ar}}) = \frac{2}{1 + \text{Erf}\left(\frac{y_{\text{ion}}^{\text{Ar}}}{\sqrt{2}\sigma_{\text{Ar}}}\right)} \frac{1}{\sqrt{2\pi}\sigma_{\text{Ar}}} \exp\left[-\frac{(y_{\text{rec}}^{\text{Ar}} - y_{\text{ion}}^{\text{Ar}})^2}{2\sigma_{\text{Ar}}^2}\right], \quad (\text{A.55})$$

with the width  $\sigma_{\text{Ar}}$  given by

$$\sigma_{\text{Ar}} = \frac{0.58 y_{\text{ion}}^{\text{Ar}}}{\sqrt{(y_{\text{ion}}^{\text{Ar}} E_{\text{max}}^{\text{Ar}})}} \quad (\text{A.56})$$

where again  $E_{\text{max}}^{\text{Ar}} = 150$  is given in keV.

Finally, the detector efficiency is parametrised by

$$A_{\text{eff}}^{\text{Ar}} = 0.96 \times (1 - \exp[a_{\text{Ar}} + b_{\text{Ar}} y_{\text{rec}}^{\text{Ar}} + c_{\text{Ar}} (y_{\text{rec}}^{\text{Ar}})^2 + d_{\text{Ar}} (y_{\text{rec}}^{\text{Ar}})^3]) \quad (\text{A.57})$$

where  $a_{\text{Ar}} = 0.336174$ ,  $b_{\text{Ar}} = -48.2704$ ,  $c_{\text{Ar}} = 301.634$ ,  $d_{\text{Ar}} = -4155.7$ .

As a consistency check we have verified that integrating the nuclear recoil spectrum in the range 1.1 keV<sub>ee</sub> (which is where the efficiency goes to zero) to 120.0 keV<sub>ee</sub> we get the expected number of recoils in the standard model with the COHERENT set up to be 132 which is in good agreement with the value  $128 \pm 17$  given by the COHERENT collaboration. For comparison, the observed number of CE $\nu$ NS events by COHERENT is  $159 \pm 43$ .

## A.2 Caesium Iodine

Here we use  $N_{\text{POT}} = 3.2 \times 10^{23}$ ,  $r = 0.0848$ ,  $L=19.3$  m,  $N = 76$ ,  $Z = 54$ , and  $m_{\text{det}} = 14.6$  kg. The QF is given by

$$\text{QF}_{\text{CsI}} = 0.0554628 + 4.30681(y E_{\text{max}}^{\text{CsI}}) - 111.707(y E_{\text{max}}^{\text{CsI}})^2 + 840.384(y E_{\text{max}}^{\text{CsI}})^3 \quad (\text{A.58})$$

where  $E_{\text{max}}^{\text{CsI}} = 0.04642$  is given in MeV. The fractional ionisation energy, then becomes

$$y_{\text{ion}}^{\text{CsI}} = \text{QF}_{\text{CsI}} y \quad (\text{A.59})$$

and the energy resolution is given by

$$R_{\text{CsI}}(\text{PE}, y_{\text{ion}}^{\text{CsI}}) = \frac{(a_{\text{CsI}}(1 + b_{\text{CsI}}))^{(1+b_{\text{CsI}})}}{\Gamma(1 + b_{\text{CsI}})} (\text{PE})^{b_{\text{CsI}}} \exp[-a_{\text{CsI}}(1 + b_{\text{CsI}})\text{PE}] \quad (\text{A.60})$$

where PE is the number of photo electrons,  $a_{\text{CsI}} = 0.0749/(y_{\text{ion}}^{\text{CsI}} E_{\text{max}}^{\text{CsI}}) = 0.00161/y_{\text{ion}}^{\text{CsI}}$  and  $b_{\text{CsI}} = 9.56(y_{\text{ion}}^{\text{CsI}} E_{\text{max}}^{\text{CsI}}) = 444 y_{\text{ion}}^{\text{CsI}}$  using  $E_{\text{max}}^{\text{CsI}} = 46.42$  in keV.

The detector efficiency is parametrised by

$$A_{\text{eff}}^{\text{CsI}} = \left( \frac{a_{\text{CsI}}^{\text{PE}}}{1 + \exp[-b_{\text{CsI}}^{\text{PE}}(\text{PE} - c_{\text{CsI}}^{\text{PE}})]} + d_{\text{CsI}}^{\text{PE}} \right) \frac{a_{\text{CsI}}^{\text{t}} + \int_{a_{\text{CsI}}^{\text{t}}}^{c_{\text{CsI}}^{\text{t}}} \exp[-b_{\text{CsI}}^{\text{t}}(t - a_{\text{CsI}}^{\text{t}})] dt}{c_{\text{CsI}}^{\text{t}}} \quad (\text{A.61})$$

where  $a_{\text{CsI}}^{\text{PE}} = 1.32045$ ,  $b_{\text{CsI}}^{\text{PE}} = 0.285979$ ,  $c_{\text{CsI}}^{\text{PE}} = 10.8646$ , and  $d_{\text{CsI}}^{\text{PE}} = -0.33332$  whereas  $a_{\text{CsI}}^{\text{t}} = 0.52 \mu\text{s}$ ,  $b_{\text{CsI}}^{\text{t}} = 0.0494 (\mu\text{s})^{-1}$ , and  $c_{\text{CsI}}^{\text{t}} = 6.0 \mu\text{s}$ . Thus, for simplicity we integrate over all times.

Again as a consistency check, integrating the nuclear recoil spectrum in the range 8 PE (which is essentially where the efficiency goes to zero) to 60 PE we get the expected number of recoils in the standard model with the COHERENT set up to be 335 which is in good agreement with the value  $341 \pm 11 \pm 42$  given by COHERENT. For comparison, the observed number of CE $\nu$ NS events by COHERENT is  $306 \pm 20$ .

### A.3 Germanium

When analysing the germanium data we use  $N_{\text{POT}} m_{\text{det}} = 2.09 \times 10^{23} \text{ kg}$ ,  $r = 0.288/3$ ,  $L=19.2 \text{ m}$ ,  $N = 40.6$ , and  $Z = 32$ . For the QF, the Lindhard model, with  $k = 0.157$ , is used in the same way as for the reactor data. For the intrinsic resolution of the detector we use  $\sigma_n(\text{SNS}) = 50.1 \text{ eV}_{\text{ee}}$  and the resolution is given by Eq. (3.38).

Integrating the nuclear recoil spectrum in the range  $1.5 \text{ keV}_{\text{ee}}$  to  $8.5 \text{ keV}_{\text{ee}}$  and  $11.0 \text{ keV}_{\text{ee}}$  to  $20.0 \text{ keV}_{\text{ee}}$  we get the expected number of recoils in the standard model with the COHERENT set up to be 34.4 which is in good agreement with the value 35.1 given by the collaboration. The observed number of CE $\nu$ NS events by COHERENT is  $20.6_{-6.3}^{+7.1}$ .

## References

- [1] D. Akimov *et al.* [COHERENT], *Science* **357** (2017) no.6356, 1123-1126 [arXiv:1708.01294 [nucl-ex]].
- [2] J. Colaresi, J. I. Collar, T. W. Hossbach, C. M. Lewis and K. M. Yocum, *Phys. Rev. Lett.* **129** (2022) no.21, 211802 [arXiv:2202.09672 [hep-ex]].
- [3] N. Ackermann, H. Bonet, A. Bonhomme, C. Buck, K. Fülber, J. Hakenmüller, J. Hempfling, G. Heusser, M. Lindner and W. Maneschg, *et al.* *Nature* **643** (2025) no.8074, 1229-1233 [arXiv:2501.05206 [hep-ex]].
- [4] A. J. Krasznahorkay, M. Csatlós, L. Csige, Z. Gácsi, J. Gulyás, M. Hunyadi, T. J. Ketel, A. Krasznahorkay, I. Kuti and B. M. Nyakó, *et al.* *Phys. Rev. Lett.* **116** (2016) no.4, 042501 [arXiv:1504.01527 [nucl-ex]].
- [5] N. J. Sas, A. J. Krasznahorkay, M. Csatlós, J. Gulyás, B. Kertész, A. Krasznahorkay, J. Molnár, I. Rajta, J. Timár and I. Vajda, *et al.* [arXiv:2205.07744 [nucl-ex]].
- [6] A. J. Krasznahorkay, M. Csatlós, L. Csige, J. Gulyás, T. J. Ketel, A. Krasznahorkay, I. Kuti, Á. Nagy, B. M. Nyakó and N. Sas, *et al.* *EPJ Web Conf.* **142**, 01019 (2017)
- [7] A. J. Krasznahorkay, M. Csatlós, L. Csige, J. Gulyás, M. Hunyadi, T. J. Ketel, A. Krasznahorkay, I. Kuti, Á. Nagy and B. M. Nyakó, *et al.* *PoS BORMIO2017*, 036 (2017)

- [8] A. J. Krasznahorkay, M. Csatlós, L. Csige, J. Gulyás, M. Hunyadi, T. J. Ketel, A. Krasznahorkay, I. Kuti, Á. Nagy and B. M. Nyakó, *et al.* EPJ Web Conf. **137**, 08010 (2017)
- [9] A. J. Krasznahorkay, M. Csatlós, L. Csige, Z. Gácsi, J. Gulyás, Á. Nagy, N. Sas, J. Timár, T. G. Tornyai and I. Vajda, *et al.* J. Phys. Conf. Ser. **1056**, no.1, 012028 (2018)
- [10] A. J. Krasznahorkay, M. Csatlós, L. Csige, J. Gulyás, M. Koszta, B. Szihalmi, J. Timár, D. S. Firak, Á. Nagy and N. J. Sas, *et al.* [arXiv:1910.10459 [nucl-ex]].
- [11] A. J. Krasznahorkay, M. Csatlós, L. Csige, J. Gulyás, A. Krasznahorkay, B. M. Nyakó, I. Rajta, J. Timár, I. Vajda and N. J. Sas, Phys. Rev. C **104**, no.4, 044003 (2021) [arXiv:2104.10075 [nucl-ex]].
- [12] A. J. Krasznahorkay, A. Krasznahorkay, M. Begala, M. Csatlós, L. Csige, J. Gulyás, A. Krakó, J. Timár, I. Rajta and I. Vajda, *et al.* Phys. Rev. C **106**, no.6, L061601 (2022) [arXiv:2209.10795 [nucl-ex]].
- [13] A. J. Krasznahorkay, A. Krasznahorkay, M. Csatlós, J. Timár, M. Begala, A. Krakó, I. Rajta, I. Vajda and N. J. Sas, Universe **10**, no.11, 409 (2024) [arXiv:2409.16300 [nucl-ex]].
- [14] J. Gulyás, T. J. Ketel, A. J. Krasznahorkay, M. Csatlós, L. Csige, Z. Gácsi, M. Hunyadi, A. Krasznahorkay, A. Vitéz and T. G. Tornyai, Nucl. Instrum. Meth. A **808**, 21-28 (2016) [arXiv:1504.00489 [nucl-ex]].
- [15] T. Anh, T. D. Trong, A. J. Krasznahorkay, A. Krasznahorkay, J. Molnár, Z. Pintye, N. A. Viet, N. Nghia, D. T. K. Linh and B. T. Hoa, *et al.* Universe **10**, no.4, 168 (2024) [arXiv:2401.11676 [nucl-ex]].
- [16] F. Bossi *et al.* [PADME], JHEP **11** (2025), 007 [arXiv:2505.24797 [hep-ex]].
- [17] K. Afanaciev *et al.* [MEG II], Eur. Phys. J. C **85**, no.7, 763 (2025) [arXiv:2411.07994 [nucl-ex]].
- [18] D. S. M. Alves, D. Barducci, G. Cavoto, L. Darmé, L. Delle Rose, L. Doria, J. L. Feng, A. Frankenthal, A. Gasparian and E. Goudzovski, *et al.* Eur. Phys. J. C **83**, no.3, 230 (2023)
- [19] J. L. Feng, B. Fornal, I. Galon, S. Gardner, J. Smolinsky, T. M. P. Tait and P. Tanedo, Phys. Rev. Lett. **117**, no.7, 071803 (2016) [arXiv:1604.07411 [hep-ph]].
- [20] J. L. Feng, B. Fornal, I. Galon, S. Gardner, J. Smolinsky, T. M. P. Tait and P. Tanedo, Phys. Rev. D **95**, no.3, 035017 (2017) [arXiv:1608.03591 [hep-ph]].
- [21] U. Ellwanger and S. Moretti, JHEP **11**, 039 (2016) [arXiv:1609.01669 [hep-ph]].
- [22] J. L. Feng, T. M. P. Tait and C. B. Verhaaren, Phys. Rev. D **102**, no.3, 036016 (2020) [arXiv:2006.01151 [hep-ph]].
- [23] T. Nomura and P. Sanyal, JHEP **05**, 232 (2021) [arXiv:2010.04266 [hep-ph]].
- [24] O. Seto and T. Shimomura, JHEP **04**, 025 (2021) [arXiv:2006.05497 [hep-ph]].
- [25] J. Kozaczuk, D. E. Morrissey and S. R. Stroberg, Phys. Rev. D **95**, no.11, 115024 (2017) [arXiv:1612.01525 [hep-ph]].

- [26] L. Delle Rose, S. Khalil, S. J. D. King and S. Moretti, *Front. in Phys.* **7**, 73 (2019) [arXiv:1812.05497 [hep-ph]].
- [27] L. Delle Rose, S. Khalil, S. J. D. King, S. Moretti and A. M. Thabt, [arXiv:1905.05031 [hep-ph]].
- [28] L. Di Luzio, P. Paradisi and N. Selimovic, [arXiv:2504.14014 [hep-ph]].
- [29] J. R. Batley *et al.* [NA48/2], *Phys. Lett. B* **746** (2015), 178-185 [arXiv:1504.00607 [hep-ex]].
- [30] D. Banerjee *et al.* [NA64], *Phys. Rev. D* **101** (2020) no.7, 071101 [arXiv:1912.11389 [hep-ex]].
- [31] X. Zhang and G. A. Miller, *Phys. Lett. B* **813** (2021), 136061 doi:10.1016/j.physletb.2021.136061 [arXiv:2008.11288 [hep-ph]].
- [32] D. Barducci and C. Toni, *JHEP* **02** (2023), 154 [erratum: *JHEP* **07** (2023), 168] [arXiv:2212.06453 [hep-ph]].
- [33] P. B. Denton and J. Gehrlein, *Phys. Rev. D* **108** (2023) no.1, 015009 [arXiv:2304.09877 [hep-ph]].
- [34] L. Delle Rose, S. Khalil and S. Moretti, *Phys. Rev. D* **96**, no.11, 115024 (2017) [arXiv:1704.03436 [hep-ph]].
- [35] L. Delle Rose, S. Khalil, S. J. D. King and S. Moretti, *Phys. Rev. D* **101**, no.11, 115009 (2020) [arXiv:1903.11146 [hep-ph]].
- [36] B. Barman, P. Ghosh, A. Ghoshal and L. Mukherjee, *JCAP* **08**, no.08, 049 (2022) [arXiv:2112.12798 [hep-ph]].
- [37] A. Bodas, R. Coy and S. J. D. King, *Eur. Phys. J. C* **81**, no.12, 1065 (2021) [arXiv:2102.07781 [hep-ph]].
- [38] P. Fayet, *Phys. Rev. D* **103**, no.3, 035034 (2021) [arXiv:2010.04673 [hep-ph]].
- [39] C. Hati, J. Kriewald, J. Orloff and A. M. Teixeira, *JHEP* **07**, 235 (2020) [arXiv:2005.00028 [hep-ph]].
- [40] X. Zhang and G. A. Miller, *Phys. Lett. B* **773**, 159-165 (2017) [arXiv:1703.04588 [nucl-th]].
- [41] B. Koch, *Nucl. Phys. A* **1008**, 122143 (2021) [arXiv:2003.05722 [hep-ph]].
- [42] H. X. Chen, [arXiv:2006.01018 [hep-ph]].
- [43] A. Aleksejevs, S. Barkanova, Y. G. Kolomensky and B. Sheff, [arXiv:2102.01127 [hep-ph]].
- [44] V. Kubarovskiy, J. R. West and S. J. Brodsky, *Phys. Rev. C* **111**, no.2, 024320 (2025) [arXiv:2206.14441 [hep-ph]].
- [45] A. C. Hayes, J. L. Friar, G. M. Hale and G. T. Garvey, *Phys. Rev. C* **105**, no.5, 055502 (2022) [arXiv:2106.06834 [nucl-th]].
- [46] M. Viviani, E. Filandri, L. Girlanda, C. Gustavino, A. Kievsky, L. E. Marcucci and R. Schiavilla, *Phys. Rev. C* **105**, no.1, 014001 (2022) [arXiv:2104.07808 [nucl-th]].

- [47] Y. Hiçyılmaz, S. Khalil and S. Moretti, Phys. Rev. D **107** (2023), no.3, 035030 [arXiv:2209.09226 [hep-ph]].
- [48] L. Delle Rose, S. Khalil, S. J. D. King, S. Moretti and A. M. Thabt, Phys. Rev. D **99** (2019) no.5, 055022 [arXiv:1811.07953 [hep-ph]].
- [49] B. Pulçiç, Chin. J. Phys. **71**, 506-517 (2021) [arXiv:1911.10482 [hep-ph]].
- [50] M. H. Fieg, T. Mäkelä, T. M. P. Tait and M. Toman, [arXiv:2602.11263 [hep-ph]].
- [51] P. S. Bhupal Dev, K. S. Babu, P. B. Denton, P. A. N. Machado, C. A. Argüelles, J. L. Barrow, S. S. Chatterjee, M. C. Chen, A. de Gouvêa and B. Dutta, *et al.* SciPost Phys. Proc. **2** (2019), 001 [arXiv:1907.00991 [hep-ph]].
- [52] M. Deniz *et al.* [TEXONO], Phys. Rev. D **81** (2010), 072001 [arXiv:0911.1597 [hep-ex]].
- [53] S. Bilmis, I. Turan, T. M. Aliev, M. Deniz, L. Singh and H. T. Wong, Phys. Rev. D **92** (2015) no.3, 033009 [arXiv:1502.07763 [hep-ph]].
- [54] R. Abbasi *et al.*, Phys. Rev. D **104** (2021) no.7, 072006 [arXiv:2106.07755 [hep-ex]].
- [55] R. Enberg, Y. Hiçyılmaz, S. Moretti, C. Pérez de los Heros and H. Waltari, JHEP **06** (2025), 182 [arXiv:2404.04717 [hep-ph]].
- [56] A. Chattaraj, A. Majumdar, D. K. Papoulias and R. Srivastava, [arXiv:2501.12443 [hep-ph]].
- [57] J. Cederkäll, Y. Hiçyılmaz, E. Lytken, S. Moretti and J. Rathsman, JHEP **12**, 027 (2025) [arXiv:2509.15128 [hep-ph]].
- [58] J. Cederkäll, Y. Hiçyılmaz, E. Lytken, S. Moretti and J. Rathsman, in “Report of the Workshop on Fundamental Nuclear and Particle Physics at the ESS Workshop”, 15-17 January 2025, Lund (Sweden) [2506.22682 [nucl-ex]].
- [59] D. Akimov *et al.* [COHERENT], Phys. Rev. Lett. **126** (2021) no.1, 012002 [arXiv:2003.10630 [nucl-ex]].
- [60] D. Akimov *et al.* [COHERENT], [arXiv:2006.12659 [nucl-ex]].
- [61] D. Akimov *et al.* [COHERENT], Phys. Rev. Lett. **129** (2022) no.8, 081801 [arXiv:2110.07730 [hep-ex]].
- [62] D. Akimov *et al.* [COHERENT], [arXiv:2307.10208 [physics.ins-det]].
- [63] S. Adamski *et al.* [COHERENT], Phys. Rev. Lett. **134**, 231801 [arXiv:2406.13806 [hep-ex]].
- [64] D. Z. Freedman, Phys. Rev. D **9** (1974), 1389-1392
- [65] M. Cadeddu, F. Dordei, C. Giunti, Y. F. Li and Y. Y. Zhang, Phys. Rev. D **101** (2020) no.3, 033004 [arXiv:1908.06045 [hep-ph]].
- [66] M. Lindner, W. Rodejohann and X. J. Xu, JHEP **03** (2017), 097 [arXiv:1612.04150 [hep-ph]].

- [67] M. Abdullah, J. B. Dent, B. Dutta, G. L. Kane, S. Liao and L. E. Strigari, *Phys. Rev. D* **98** (2018) no.1, 015005 [arXiv:1803.01224 [hep-ph]].
- [68] L. J. Flores, N. Nath and E. Peinado, *JHEP* **06** (2020), 045 [arXiv:2002.12342 [hep-ph]].
- [69] M. Cadeddu, N. Cargioli, F. Dordei, C. Giunti, Y. F. Li, E. Picciau and Y. Y. Zhang, *JHEP* **01** (2021), 116 [arXiv:2008.05022 [hep-ph]].
- [70] H. Banerjee, B. Dutta and S. Roy, *Phys. Rev. D* **104** (2021) no.1, 015015 [arXiv:2103.10196 [hep-ph]].
- [71] M. Atzori Corona, M. Cadeddu, N. Cargioli, F. Dordei, C. Giunti, Y. F. Li, E. Picciau, C. A. Ternes and Y. Y. Zhang, *JHEP* **05** (2022), 109 [arXiv:2202.11002 [hep-ph]].
- [72] P. Coloma, I. Esteban, M. C. Gonzalez-Garcia, L. Larizgoitia, F. Monrabal and S. Palomares-Ruiz, *JHEP* **05** (2022), 037 [arXiv:2202.10829 [hep-ph]].
- [73] M. Atzori Corona, M. Cadeddu, N. Cargioli, F. Dordei, C. Giunti, Y. F. Li, C. A. Ternes and Y. Y. Zhang, *JHEP* **09** (2022), 164 [arXiv:2205.09484 [hep-ph]].
- [74] A. Chattaraj, A. Majumdar and R. Srivastava, *Phys. Lett. B* **864** (2025), 139438 [arXiv:2501.12441 [hep-ph]].
- [75] V. De Romeri, D. K. Papoulias and G. Sanchez Garcia, *Phys. Rev. D* **111** (2025) no.7, 7 [arXiv:2501.17843 [hep-ph]].
- [76] M. Atzori Corona, M. Cadeddu, N. Cargioli, F. Dordei and C. Giunti, *Phys. Rev. D* **112** (2025) no.1, 015007 [arXiv:2501.18550 [hep-ph]].
- [77] M. Atzori Corona, M. Cadeddu, N. Cargioli, G. Co', F. Dordei and C. Giunti, *Phys. Lett. B* **869** (2025), 139856 [arXiv:2506.13555 [hep-ph]].
- [78] Y. Li, G. Herrera and P. Huber, *JHEP* **11** (2025), 022 [arXiv:2502.12308 [hep-ph]].
- [79] E. Aprile *et al.* [XENON], *Phys. Rev. Lett.* **133** (2024) no.19, 191002 [arXiv:2408.02877 [hep-ex]].
- [80] Z. Bo *et al.* [PandaX], *Phys. Rev. Lett.* **133** (2024) no.19, 191001 [arXiv:2407.10892 [hep-ex]].
- [81] M. Atzori Corona, M. Cadeddu, N. Cargioli, F. Dordei and M. Sestu, [arXiv:2509.22178 [hep-ph]].
- [82] V. De Romeri, A. Majumdar, D. K. Papoulias and R. Srivastava, [arXiv:2512.08853 [hep-ph]].
- [83] P. B. Denton and J. Gehrlein, *Phys. Rev. D* **106** (2022) no.1, 015022 doi:10.1103/PhysRevD.106.015022 [arXiv:2204.09060 [hep-ph]].
- [84] M. Cadeddu, F. Dordei and C. Giunti, *EPL* **143** (2023) no.3, 34001 [arXiv:2307.08842 [hep-ph]].
- [85] S. Karmakar *et al.* [TEXONO], *Phys. Rev. Lett.* **134** (2025) no.12, 12 [arXiv:2411.18812 [nucl-ex]].

- [86] I. Alekseev *et al.* [ $\nu$ GeN], Phys. Rev. D **106** (2022) no.5, L051101 [arXiv:2205.04305 [nucl-ex]].
- [87] G. Angloher *et al.* [NUCLEUS], Eur. Phys. J. C **79** (2019) no.12, 1018 [arXiv:1905.10258 [physics.ins-det]].
- [88] J. J. Choi *et al.* [NEON], Eur. Phys. J. C **83** (2023) no.3, 226 [arXiv:2204.06318 [hep-ex]].
- [89] A. Aguilar-Arevalo *et al.* [CONNIE], JHEP **05** (2022), 017 [arXiv:2110.13033 [hep-ex]].
- [90] C. Coriano, L. Delle Rose and C. Marzo, JHEP **02** (2016), 135 doi:10.1007/JHEP02(2016)135 [arXiv:1510.02379 [hep-ph]].
- [91] P. Abreu *et al.* [DELPHI], Z. Phys. C **65**, 603-618 (1995).
- [92] J. Erler, P. Langacker, S. Munir and E. Rojas, JHEP **08**, 017 (2009) [arXiv:0906.2435 [hep-ph]].
- [93] W. Porod, Comput. Phys. Commun. **153**, 275-315 (2003) [arXiv:hep-ph/0301101 [hep-ph]].
- [94] W. Porod and F. Staub, Comput. Phys. Commun. **183**, 2458-2469 (2012) [arXiv:1104.1573 [hep-ph]].
- [95] J. Braathen, M. D. Goodsell and F. Staub, Eur. Phys. J. C **77**, no.11, 757 (2017) [arXiv:1706.05372 [hep-ph]].
- [96] F. Staub, Comput. Phys. Commun. **185**, 1773-1790 (2014) [arXiv:1309.7223 [hep-ph]].
- [97] F. Staub, Adv. High Energy Phys. **2015**, 840780 (2015) [arXiv:1503.04200 [hep-ph]].
- [98] S. Navas *et al.* [Particle Data Group], Phys. Rev. D **110** (2024) no.3, 030001
- [99] G. Aad *et al.* [ATLAS], Phys. Lett. B **842** (2023), 137963 [arXiv:2301.10731 [hep-ex]].
- [100] Y. Amhis *et al.* [HFLAV], [arXiv:1207.1158 [hep-ex]].
- [101] R. Aaij *et al.* [LHCb], Phys. Rev. Lett. **110**, no.2, 021801 (2013) [arXiv:1211.2674 [hep-ex]].
- [102] D. Asner *et al.* [HFLAV], [arXiv:1010.1589 [hep-ex]].
- [103] R. Aliberti, T. Aoyama, E. Balzani, A. Bashir, G. Benton, J. Bijnens, V. Biloshytskyi, T. Blum, D. Boito and M. Bruno, *et al.* [arXiv:2505.21476 [hep-ph]].
- [104] D. P. Aguillard *et al.* [Muon g-2], Phys. Rev. Lett. **135** (2025) no.10, 101802 [arXiv:2506.03069 [hep-ex]].
- [105] L. Morel, Z. Yao, P. Cladé and S. Guellati-Khélifa, Nature **588** (2020) no.7836, 61-65.
- [106] P. L. Anthony *et al.* [SLAC E158], Phys. Rev. Lett. **95** (2005), 081601 [arXiv:hep-ex/0504049 [hep-ex]].
- [107] Y. Kahn, G. Krnjaic, S. Mishra-Sharma and T. M. P. Tait, JHEP **05** (2017), 002 [arXiv:1609.09072 [hep-ph]].

- [108] S. G. Porsev, K. Beloy and A. Derevianko, Phys. Rev. Lett. **102** (2009), 181601 [arXiv:0902.0335 [hep-ph]].
- [109] G. Arcadi, M. Lindner, J. Martins and F. S. Queiroz, Nucl. Phys. B **959** (2020), 115158 [arXiv:1906.04755 [hep-ph]].
- [110] S. Klein and J. Nystrand, Phys. Rev. C **60** (1999), 014903 [arXiv:hep-ph/9902259 [hep-ph]].
- [111] V. I. Kopeikin, Phys. Atom. Nucl. **75** (2012), 143-152.
- [112] T. A. Mueller, D. Lhuillier, M. Fallot, A. Letourneau, S. Cormon, M. Fechner, L. Giot, T. Lasserre, J. Martino and G. Mention, *et al.* Phys. Rev. C **83** (2011), 054615 [arXiv:1101.2663 [hep-ex]].
- [113] P. Huber, Phys. Rev. C **84** (2011), 024617 [erratum: Phys. Rev. C **85** (2012), 029901] [arXiv:1106.0687 [hep-ph]].
- [114] F. P. An *et al.* [Daya Bay], Phys. Rev. Lett. **129** (2022) no.4, 041801 [arXiv:2203.06686 [hep-ex]].
- [115] F. P. An *et al.* [Daya Bay], Chin. Phys. C **45** (2021) no.7, 073001 [arXiv:2102.04614 [hep-ex]].
- [116] J. I. Collar, A. R. L. Kavner and C. M. Lewis, Phys. Rev. D **103** (2021) no.12, 122003 [arXiv:2102.10089 [nucl-ex]].
- [117] M. Adhikari, M. Ahn, D. Amaya Matamoros, P. S. Barbeau, V. Belov, I. Bernardi, C. Bock, A. Bolozdynya, R. Bouabid and A. Bracho, *et al.* [arXiv:2603.17951 [hep-ex]].